Comparison of the mechanism of antimicrobial action of the gold(I) compound auranofin in Gram-positive and Gram-negative bacteria

Laísa Quadros Barsé[1*], Agnes Ulfig[1,5*], Marharyta Varatnitskaya[1], Melissa Vázquez-Hernández[3], Jihyun Yoo[1], Astrid M. Imann[1,2], Natalie Lupilov[1], Marina Fischer[4], Katja Becker[4], Julia E. Bandow[3], and Lars I. Leichert[1†]

[1] Ruhr University Bochum, Medical Faculty, Institute of Biochemistry and Pathobiochemistry – Microbial Biochemistry, Universitätsstrasse 150, 44780 Bochum, Germany

[2] Westphalian University of Applied Sciences, Institute of Electrical Engineering and Applied Sciences – Molecular Biology, August-Schmidt-Ring 10, 45665 Recklinghausen, Germany

[3] Ruhr University Bochum, Faculty of Biology and Biotechnology, Applied Microbiology, Universitätsstrasse 150, 44780 Bochum, Germany

[4] Justus Liebig University Giessen, Chair of Biochemistry and Molecular Biology, Interdisciplinary Research Center, Heinrich-Buff-Ring 26-32, 35392 Giessen, Germany

[5] Current address: University of Iceland, Faculty of Medicine, Louma G. Laboratory of Epigenetic Research, Sturlugata 8, 101 Reykjavik, Iceland

[*] Shared first authorship.

[†]Correspondence: Lars I. Leichert
Ruhr University Bochum
Institute of Biochemistry and Pathobiochemistry
Microbial Biochemistry
Universitätsstrasse 150
44780 Bochum, Germany
Phone: +49 234 3224585
Fax: +49 234 3214332
E-mail: lars.leichert@ruhr-uni-bochum.de

KEYWORDS: auranofin, gold, drug repurposing, thioredoxin reductase, proteomics, *Escherichia coli*, *Bacillus subtilis*

ABSTRACT

The antirheumatic gold(I) compound auranofin has been suggested to exhibit bactericidal activity by disrupting the thiol homeostasis through direct inhibition of bacterial thioredoxin reductase (TrxB). While highly effective at killing Gram-positive bacteria, it lacks significant activity against Gram-negative species for reasons that largely remain unclear. Here, we aimed to elucidate the molecular mechanisms underlying the low susceptibility of the Gram-negative model organism *Escherichia coli* to auranofin when compared to the Gram-positive model organism *Bacillus subtilis*. A change in the proteome of *E. coli* exposed to auranofin suggested that the effect of this gold compound is a combination of inactivation of thiol-containing enzymes, upregulation of proteins involved in basal metabolism, and the consequent induction of systemic oxidative stress. Susceptibility tests in *E. coli* mutants lacking the proteins upregulated upon auranofin treatment suggested that none of them are directly involved in *E. coli*'s high tolerance to auranofin. To elucidate factors that could make Gram-negative bacteria less susceptible to auranofin, we tested *E. coli* cells lacking the efflux pump component TolC. These cells were more sensitive to auranofin treatment than the wild type, but not to an extent that would fully explain the observed difference in susceptibility of Gram-positive and Gram-negative organisms. We thus tested if *E. coli*'s thioredoxin reductase (TrxB) is inherently less sensitive to auranofin than TrxB from *B. subtilis*, which was not the case. *E. coli* cells lacking components of the thioredoxin-system were also only marginally more susceptible to auranofin. However, *E. coli* strains lacking the low molecular weight thiol glutathione, but not glutathione reductase, showed a high susceptibility to auranofin. Bacterial cells expressing the genetically encoded redox probe roGFP2 allowed us to observe the oxidation of cellular protein thiols *in situ*. In line with their susceptibility, the kinetics of probe oxidation and the degree of oxidation promoted by auranofin is significantly higher in Gram-positive bacteria when compared to Gram-negative bacteria. Based on our findings, we hypothesize that auranofin leads to a global disturbance in the cellular thiol redox homeostasis in bacteria, but Gram-negative bacteria are inherently more resistant due to the presence of drug export systems and high cellular concentrations of glutathione.

INTRODUCTION

The evolutionary emergence and rapid spread of multidrug-resistant pathogenic bacteria is an ongoing and rising public health concern, as infections caused by these pathogens claim the lives of nearly 700,000 people across the globe each year (Humphreys and Fleck, 2016). This number is expected to increase dramatically if no urgent actions are taken. Unfortunately, the slow progress in the discovery and development of new antibiotic classes has led to a limited availability of novel antimicrobial compounds for clinical use and, thus, made the effective treatment of many bacterial infections more challenging (Hutchings et al., 2019). Accordingly, there is an urgent medical need to identify new and improved antibacterial agents with unprecedented modes of action to tackle the global antibiotic resistance crisis (Aslam et al., 2018). Since conventional *de novo* drug discovery and development are lengthy, expensive, and complex, repurposing approved drugs for antimicrobial therapy by re-evaluating their biological targets and mechanisms of action is considered a key strategy to overcome these issues (Farha and Brown, 2019). Although using known drugs for indications they were not originally developed for is far from new, it has gained considerable attention in the last decade, with about one-third of new US Food and Drug Administration (FDA) approvals being for repurposed drugs (Cha et al., 2018).

The use of metals, such as silver, gold, and platinum, and compounds based on these and other metals, in treating diseases dates to ancient times (Wang et al., 2012), but their full potential as therapeutic drugs has not been realized yet. With the discovery of the platinum-based compound cisplatin as an anticancer agent in the 20th century, metallodrugs have experienced an impressive renaissance of interest in modern medicine, leading to the development of several other metal complexes with antitumor and anti-inflammatory properties over the last decades (Alderden et al., 2006).

Auranofin, a gold(I)-containing triethyl phosphine, was initially approved by the FDA in 1985 as an anti-inflammatory drug for the treatment of rheumatoid arthritis and was the first orally active gold compound proven to slow the progression of the disease by inhibiting antibody-mediated cellular toxicity and stimulating cell-mediated immunity (Finkelstein et al., 1976; Messori and Marcon, 2004). Auranofin's primary mode of action in humans is thought to be the inhibition of thioredoxin reductase (TrxR) (Gromer et al. 1998). Auranofin's exceptionally high affinity toward TrxR is due to the reactivity of its thiol ligand with thiol groups and especially the selenol group of the selenocysteine present in eukaryotic TrxR (Angelucci et al., 2009; Jeon et al., 2003; Rackham et al., 2011; Saccoccia et al., 2012). TrxR was shown to be highly expressed in the inflamed joints of patients with rheumatoid arthritis, and it is assumed to be involved in disease activity and suppression of apoptosis in the affected

92 tissue (Kabuyama et al., 2008; Maurice et al., 1999). TrxR is a central component of the
93 antioxidant thioredoxin (Trx) system. It catalyzes the NADPH-dependent reduction of the
94 redox protein thioredoxin (Trx), which is crucial in maintaining the cellular environment in a
95 reduced state and protecting the cells against damage from oxidative stress (Holmgren and
96 Björnstedt, 1995; Lu and Holmgren, 2014).

97 More recent studies also indicate that TrxR is highly abundant in various types of human
98 cancer cells and, thus, represents a promising therapeutic target for anticancer drug
99 development. Gold-induced inactivation of mammalian TrxR by auranofin leads to severe
100 oxidative stress due to the overproduction of reactive oxygen species (ROS) and activation
101 of apoptotic signaling pathways, ultimately triggering cancer cell death (Bian et al., 2019;
102 Hwang-Bo et al., 2017).

103 Besides these effects in eukaryotes, auranofin, and related gold-based compounds have
104 also shown promising activity against a wide range of pathogenic microorganisms at a
105 clinically achievable nanomolar range. In a study by Debnath et al., auranofin was highly
106 efficacious against the intestinal parasite *Entamoeba histolytica,* providing the first evidence
107 that this gold drug could be repurposed as a novel antimicrobial agent (Debnath et al., 2012).
108 Indeed, more recent studies have reported remarkable bactericidal effects of auranofin
109 against various pathogenic Gram-positive bacteria *in vitro* and *in vivo*, including
110 *Mycobacterium tuberculosis*, certain *Bacillus* spp., *Enterococcus faecalis,* and methicillin-
111 resistant *Staphylococcus aureus* (MRSA) (Aguinagalde et al., 2015; Cassetta et al., 2014;
112 Harbut et al., 2015; Hokai et al., 2014). As a result, auranofin has become the reference
113 compound for developing new, structurally related organogold antimicrobial drugs with lower
114 toxicity, a broader spectrum of activity, and greater efficacy (Marzo et al., 2018).

115 Although progress has been made in understanding the underlying mechanistical aspects of
116 auranofin's antimicrobial activity, the precise mechanisms of its action and the respective
117 biological targets in bacteria are still largely unknown.

118 Recent studies point toward a complex multitarget mechanism of auranofin's action in
119 prokaryotic organisms that involves inhibition of several biosynthetic pathways, including
120 protein, DNA, and cell wall synthesis (Thangamani et al., 2016), and disruption of thiol-redox
121 homeostasis (Caroli et al., 2012; Harbut et al., 2015). Among these possible modes of action,
122 inhibition of thiol-containing redox enzymes essential for maintaining intracellular thiol-redox
123 balance is widely considered the primary mechanism through which auranofin exerts its
124 cytotoxic effects on bacteria (Harbut et al., 2015). A growing number of studies demonstrate
125 a strong inhibitory effect on bacterial thioredoxin reductase (TrxB). For instance, auranofin
126 has been shown to effectively inhibit TrxB of *S. aureus*, *M. tuberculosis,* and *H. pylori in vitro*,

127 with IC_{50} values in the low nanomolar range. Notably, the growth of these organisms was
128 also strongly impaired in the presence of auranofin (Harbut et al., 2015; Owings et al., 2016).

129 While auranofin is highly effective against Gram-positive bacteria, it is much less active
130 against Gram-negative bacteria, exhibiting a markedly higher minimal inhibitory
131 concentration (MIC) (Harbut et al., 2015). However, the reasons for the limited susceptibility
132 of Gram-negative bacteria to auranofin are still unknown.

133 In this work, we aimed to elucidate the molecular mechanisms underlying the increased
134 tolerance of Gram-negative bacteria to auranofin. We utilized *E. coli* and *B. subtilis* as
135 representative species of Gram-negative and Gram-positive bacteria, respectively, to
136 systematically uncover the mode of auranofin's action by testing its effect on TrxB activity
137 and growth of these organisms. We studied the proteomic response of *E. coli* exposed to
138 auranofin stress to uncover potential defense mechanisms that could mediate their increased
139 resistance to auranofin. We also focused on factors that differ between Gram-positive and
140 Gram-negative species, such as TolC, the outer membrane factor of an efflux pump in *E.*
141 *coli*. Cells lacking TolC were more susceptible to auranofin, however not to an extent that
142 would make TolC-dependent drug efflux the only factor explaining *E. coli*'s relative resistance
143 to auranofin. A systematic evaluation of mutants lacking components of the thioredoxin
144 system and the glutathione-dependent antioxidant system suggests that the presence of a
145 high concentration of the low molecular weight thiol glutathione is a major factor contributing
146 to *E. coli*'s tolerance. This is in line with cytoplasmic thiol oxidation caused by auranofin *in*
147 *vivo*, which we observed using *E. coli* and *B. subtilis* cells expressing the well-known redox
148 probe roGFP2. Overall, our data suggest that auranofin's mode of action against Gram-
149 negative species does not significantly differ from that against Gram-positive species.
150 Instead, it seems that the higher resistance of *E. coli* is caused in part by a combination of
151 drug efflux and, more importantly, the presence of high concentrations of the low-molecular
152 weight thiol glutathione, which attenuate the cytotoxic effects of auranofin.

153 **MATERIAL AND METHODS**

154 **Determination of the Minimal Inhibitory Concentration (MIC) of Auranofin against**
155 **Gram-negative and Gram-positive bacteria**

156 Auranofin (Santa Cruz Biotechnology, Heidelberg, Germany) was tested for bactericidal
157 activity against *Acinetobacter baumannii* DSM 30007, *Pseudomonas aeruginosa* DSM
158 50071, *Bacillus subtilis* 168, *Staphylococcus aureus* DSM 20231, *Staphylococcus aureus*
159 ATCC 43300 (MRSA), *E. coli* DSM 30083, *E. coli* BW25113 and *E. coli* BW25113-derived
160 mutant strains from the KEIO collection (Baba et al., 2006) listed in Table 1.
161 *E. coli* DSM 30083, *A. baumannii*, *S. aureus*, and *B. subtilis* were grown in Mueller Hinton
162 broth, and *P. aeruginosa* in cation-adjusted Mueller Hinton II. MIC assays with these strains
163 were performed in a microdilution assay in 200 µL medium according to CLSI guidelines, as
164 described by Albada et al. (Albada et al., 2012). *E. coli* BW25113 and the derived mutant
165 strains from the KEIO collection were grown in reaction tubes containing 5 mL MOPS
166 Minimal Medium (Teknova) (Neidhardt et al., 1974) supplemented with 10 µM thiamine.

167 Auranofin was dissolved in DMSO to a final concentration of 10 mg/mL. Serial dilutions of
168 this stock solution were prepared in the various culture media with the Tecan Freedom Evo
169 75 liquid handling workstation (Tecan, Männedorf, Switzerland) for tests according to CLSI
170 guidelines. They typically covered a range from 512 to 0.5 µg/mL. In *E. coli* BW25113 and
171 the *E. coli* BW25113-derived mutants, a range of 256 µg/mL to 4 µg/mL was tested; these
172 dilutions were prepared manually.

173 All bacterial strains were grown until the exponential growth phase was reached. At an OD_{600}
174 of 0.4-0.5, $5x10^5$ cells/mL of the exponentially growing cultures were used to inoculate the
175 previously prepared auranofin dilutions in the same growth medium. After 16-18 hours of
176 incubation at 37 °C, bacterial growth at various auranofin concentrations was assessed
177 visually and photometrically by measuring the cultures' OD at 600 nm. The lowest auranofin
178 concentration with no visually perceptible growth was recorded as MIC.

179 **Construction of plasmids encoding bacterial TrxB**

180 Plasmids and oligonucleotides used in this study are listed in Tables 1 and S1, respectively.
181 Plasmid construction followed standard procedures. The correctness of all newly constructed
182 plasmids was verified by DNA sequencing.

183 For the expression and subsequent purification of *E. coli* MG1655 and *B. subtilis* 168 TrxB,
184 the respective *trxB* genes were fused to an N-terminal SUMO tag and cloned into pET22b(+)

185 vectors (Butt et al., 2005). The SUMO tag contains a SUMO (Small Ubiquitin-like Modifier)
186 protein sequence, which enhances expression and solubility of the fusion protein, a His_6 tag,
187 which allows for purification of the fusion protein using Ni–NTA chromatography, and an Ulp1
188 protease cleavage site (Butt et al., 2005).

189 The SUMO tag sequence was amplified from the pE-SUMO plasmid using the forward primer
190 AI003_SUMO_for carrying a NdeI restriction site and AI004_SUMO_rev or
191 MM004_SUMO_rev, containing an overhang complementary to the N-terminal portion of the
192 *E. coli* or *B. subtilis trxB* sequence, respectively (Table S1). In a second PCR, the genes
193 encoding TrxB were amplified from genomic DNA of *E. coli* MG1655 and *B. subtilis* 168
194 using the following primers: AI001_for and AI002_rev, and MM001_for and MM002_rev for
195 *E. coli* and *B. subtilis*, respectively. The resulting PCR fragments contained an overhang
196 sequence to the SUMO tag at the 5' end and an XhoI restriction site at the 3' end. Finally, an
197 overlap PCR was performed using the primers AI003_SUMO_for and AI002_rev (for *E. coli*
198 TrxB) or MM002_rev (for *B. subtilis* TrxB) to fuse the SUMO tag sequence to the N-terminus
199 of the respective *trxB* gene. The obtained PCR product (i.e., NdeI-SUMO-TrxB-XhoI) was
200 then restricted with NdeI and XhoI and cloned into a pET22b(+) vector, resulting in pAI (*E.*
201 *coli* MG1655 *trxB*) and pMM (*B. subtilis* 168 *trxB*). *E. coli* DH5α and *E. coli* BL21(DE3) cells
202 were then transformed with the plasmids for plasmid maintenance and heterologous protein
203 expression, respectively.

204 **Heterologous protein expression**

205 For heterologous protein expression, a single colony of *E. coli* BL21 (DE3) carrying pAI or
206 pMM was used to inoculate 50 mL LB broth containing 200 µg/L ampicillin, and the cells
207 were grown overnight at 37 °C and 125 rpm. The overnight culture was then used to
208 inoculate 5 L of LB medium, supplemented with ampicillin. Cells were incubated at 37 °C and
209 125 rpm until an OD_{600} of 0.5-0.6 was reached. Subsequently, protein expression was
210 induced by adding 1 mM isopropyl 1-thio-ß-D-galactopyranoside (IPTG) to the cell culture.
211 After overnight incubation at 20 °C and 125 rpm, cells were harvested by centrifugation at
212 7800 x *g* and 4 °C for 45 min, and pellets were stored at -80 °C.

213 **Purification of ecTrxB and bsTrxB**

214 *E. coli* BL21 (DE3) cell pellets obtained after expression of *B. subtilis* 168 (*bs*TrxB) or
215 *E. coli* MG1655 TrxB (*ec*TrxB) and were resuspended in 30 mL lysis buffer 1 (50 mM sodium
216 phosphate, 300 mM NaCl, pH 8) containing 2 mL of EDTA-free protease inhibitor mixture
217 (Roche Applied Science, Penzberg, Germany). Cells were disrupted by passing the cell
218 suspension three times through a Constant Cell disruption system (TS benchtop; Constant

219 Systems, Daventry, UK) at 1.9 kbar and 4 °C, followed by the addition of the serine protease
220 inhibitor phenylmethylsulfonyl fluoride (PMSF) to a final concentration of 1 mM. The cell
221 lysate was centrifuged at 6700 x *g* and 4 °C for 1 h. The supernatant was vacuum filtered
222 through a 0.45 µm filter. Proteins were purified using Immobilized Metal Affinity
223 Chromatography (IMAC). The supernatant was loaded onto a Pierce Centrifuge Column pre-
224 packed with 2 mL HisPur™ Ni-NTA-Resin (Thermo Fischer Scientific) and pre-equilibrated
225 with lysis buffer 1. The column was then washed with lysis buffer 1, supplemented with 10
226 mM imidazole, followed by one washing step with lysis buffer 1 containing 20 mM imidazole.
227 Proteins were eluted by adding elution buffer 1 (50 mM sodium phosphate, 300 mM NaCl,
228 250 mM imidazole, pH 8.0). Elution fractions containing the respective protein were
229 combined, filled to 50 mL with lysis buffer 1, and concentrated to 1 mL using a Vivaspin 20
230 PES, MWCO 10000 concentrator system (Sartorius Stedim Biotech). The latter step was
231 repeated twice to reduce imidazole concentration in the buffer. To remove the SUMO tag,
232 *ec*TrxB and *bs*TrxB were digested with a His_6-tagged SUMO Ulp1 protease, using a 75-fold
233 excess (w/w) protein to protease. After overnight incubation at 4 °C, the reaction mixtures
234 were purified using IMAC as described above. Wash fractions containing the purified and
235 untagged TrxBs were concentrated using Vivaspin 20 PES, MWCO 10000 concentrator
236 system (Sartorius Stedim Biotech) to a final volume of 1 mL. Proteins were stored in lysis
237 buffer 1 supplemented with 10 % (v/v) glycerol at -80 °C.

238 **Table 1: Bacterial strains and plasmids used in this study.**

	Relevant properties	**Source/reference**
Bacterial strains		
A. baumannii DSM 30007	type strain	DSMZ (German collection of microorganisms and cell culture; Braunschweig, Germany).
B. subtilis 168	Wild type strain	DSMZ, strain DSM402
B. subtilis LQB001	*B. subtilis* 168 containing chromosomally inserted roGFP2 under the control of a xylose-inducible promotor in the *amyE* locus	This work.
E. coli DH5α	Cloning strain	New England Biolabs, Ipswich, MA, USA

E. coli BL21 (DE3)	Strain for heterologous protein expression from pET vectors	Stratagene, Santa Clara, CA.
E. coli DSM 30083	type strain	DSMZ
E. coli MG1655	Wild type strain	ATCC Manassas, VA, US, strain ATCC 700926
E. coli BW25113	Parental strain Keio collection (Baba et al., 2006)	The National BioResource Project (National Institute of Genomics, Japan)
E. coli JW5503	*E. coli* BW25113 Δ*tolC*	The National BioResource Project (National Institute of Genomics, Japan)
E. coli JW3467	*E. coli* BW25113 Δ*gor*	The National BioResource Project (National Institute of Genomics, Japan)
E. coli JW2663	*E. coli* BW25113 Δ*gshA*	The National BioResource Project (National Institute of Genomics, Japan)
E. coli JW5156	*E. coli* BW25113 Δ*trxA*	The National BioResource Project (National Institute of Genomics, Japan)
E. coli JW0871	*E. coli* BW25113 Δ*trxB*	The National BioResource Project (National Institute of Genomics, Japan)
E. coli AI001	DH5α pAI (*E. coli* trxB in pET22b(+))	This work
E. coli AI002	BL21 (DE3) pAI (E. coli trxB in pET22b(+))	This work
E. coli LQB001	BW25113 pCC_roGFP2	This work.
E. coli MM003	DH5α pMM (*B. subtilis* trxB in pET22b(+))	This work
E. coli MM004	BL21 (DE3) pMM (*B. subtilis* trxB in pET22b(+))	This work

P. aeruginosa DSM 50071	type strain	DSMZ (German collection of microorganisms and cell culture; Braunschweig, Germany).
S. aureus DSM 20231	type strain	DSM (German collection of microorganisms and cell culture; Braunschweig, Germany).
S. aureus ATCC 43300 (MRSA)	Methicillin-resistant	ATCC, Manassas, VA, US.
Plasmids		
pET22b(+)	IPTG-inducible plasmid (high copy number)	Novagen
pMM	pET22b(+) encoding *B. subtilis* 168 TrxR with an N-terminal SUMO tag	This study
pAI	pET22b(+) encoding *E. coli* MG1655 TrxR with an N-terminal SUMO tag	This study
pE-SUMO	SUMO tag	Lab collection
pCC_roGFP2	pCC encoding roGFP2. IPTG-inducible plasmid, amp^R	(Müller et al., 2017)
pSG1729_roGFP2	pSG1729 (Lewis and Marston, 1999) encodes roGFP2 under a xylose-inducible promotor for chromosomal insertion into the amyE locus of *B. subtilis*. amp^R, $spec^R$	This work
pMX_roGFP2	pMX encoding roGFP2 codon-optimized for *B. subtilis*.	Thermo Fischer Scientific

239

240 **Analysis of TrxB inhibition by auranofin using a DTNB reduction assay**

241 TrxB activity in the absence or presence of auranofin was determined by performing a 5,5'-
242 dithiobis(2-nitrobenzoic) acid (DTNB) reduction assay. In this NADPH-dependent assay,

243 TrxB reduces DTNB directly to yield the spectrophotometrically detectable 5-thio-2-
244 nitrobenzoic acid (TNB). DTNB assays were performed in transparent, flat-bottom 96-well
245 plates (Sarstedt, Nümbrecht, Germany) as described by Lu et al. (Lu et al., 2013). Briefly,
246 1 µM *ec*TrxB or *bs*TrxB were added to TE buffer (50 mM Tris-HCl, 2 mM EDTA, pH 7.5)
247 containing 200 µM NADPH (Sigma-Aldrich, St. Louis, USA) for 5 min, in a total volume of
248 100 µL. The enzymatic reaction was then initiated by adding 100 µL TE buffer containing
249 2 mM DTNB (Sigma-Aldrich, St. Louis, USA). The amount of liberated TNB was then
250 quantified spectrophotometrically by measuring the absorbance at 412 nm for 15 min.
251 Experiments containing auranofin ranging from 0.1 to 2 µM were performed in triplicate. The
252 remaining TrxB activity after adding auranofin was normalized to activity in the absence of
253 auranofin, which was set to 100 %.

254 **Proteomic profiling of auranofin-stressed *E. coli* cells using radioactive labeling and**
255 **2D-PAGE**

256 2D PAGE-based proteomic analysis was performed as previously described (Wenzel *et al.*,
257 2011). For the analysis of the proteomic response of *E. coli* to auranofin exposure,
258 *E. coli* MG1655 was used. Briefly, a stock of auranofin was dissolved in DMSO to a final
259 concentration of 10 mg/mL. *E. coli* MG1655 cells were grown in Neidhardt MOPS minimal
260 medium (Neidhardt et al., 1974) at 37 °C and 200 rpm until an OD_{500} of 0.35 was reached.
261 Cultures were split into an untreated control and a culture treated with a sublethal
262 concentration of 120 µg/mL. After 10 minutes, newly synthesized proteins were labeled with
263 0.37 MBq/mL L-[^{35}S]-methionine (Hartmann Analytic, Braunschweig, Germany). 5 min. later,
264 protein synthesis was stopped by the addition of 100 µg/mL chloramphenicol and non-
265 radioactive L-methionine (to a final concentration of 1 mM L-methionine and 10 mM Tris
266 originally set to pH 7.5 in the stock solution). Cells were harvested by centrifugation and
267 washed twice with 100 mM Tris/1 mM EDTA, pH 7.5. The cells were disrupted by
268 ultrasonication with a VialTweeter (Hielscher, Teltow, Germany), and the supernatant was
269 recovered after centrifugation. The protein concentration was determined by a Bradford
270 assay (Roti NanoQuant, Roth, Karlsruhe, Germany). Protein biosynthesis rates were
271 determined by measuring the incorporation of radioactive methionine in auranofin-treated
272 and untreated samples after protein precipitation with 20 % (w/v) trichloro acetic acid using a
273 scintillation counter (Tri-Carb 2800TR, PerkinElmer). 55 µg of protein from pulse-labeled
274 samples for analytical gels and 300 µg of protein from unlabeled samples for preparative
275 gels were rehydrated into IPG strips (24 cm, pH 4-7; GE Healthcare, Chalfont St Giles, UK).
276 A Multiphor II (GE Healthcare) was used for isoelectric focusing, and for the second
277 dimension PAGE, the Ettan DALTwelve system (GE Healthcare) was used. The gels were
278 stained with ruthenium(II)tris(4,7-diphenyl-1, 10-phenantrolin disulfonate) and washed with

279 ethanol and acetic acid (Rabilloud et al., 2001). Fluorescent gel images were taken with the
280 Typhoon Trio$^+$ Variable Mode Imager (GE Healthcare) using an excitation wavelength of 532
281 nm and an emission filter of 600 nm. Radio-labeled analytical gels were dried onto Whatman
282 paper and exposed to Storage Phospho Screens (GE Healthcare). The phosphoscreens
283 were scanned with the Typhoon Trio$^+$ with an excitation wavelength of 633 nm and an
284 emission filter of 390 nm. For visualization and analysis of the 2D gels, the Decodon Delta
285 2D image analysis software was used (Bandow et al., 2008). Two biological replicates with
286 one technical replicate each were analyzed against their respective controls for quantitation.
287 Protein spots detected as two-fold upregulated compared to the untreated control based on
288 relative signal intensity were defined as marker proteins upon visual inspection (Wenzel et
289 al., 2011).

290 Protein identification from gel spots was performed as described previously (Wenzel et al.,
291 2013). Spots were excised from a non-radioactive 2D gel and destained with 20 mM
292 ammonium bicarbonate in 30 % acetonitrile. The protein spots were digested with either
293 12.5 ng/µL trypsin for low-intensity or 6.25 ng/µL trypsin for high-intensity spots (Promega,
294 Fitchburg, FI, USA) for 18 h at 37 °C. Peptides were eluted in 0.1 % trifluoroacetic acid in
295 MS-grade water and ultrasonicated for 15 min once (or twice if they were low-intensity
296 spots). For protein identification, the samples were analyzed using a nanoACQUITY-UPLC-
297 coupled SYNAPT G2-S high-definition mass spectrometer equipped with a NanoLockSpray
298 Source for electrospray ionization and a time-of-flight detector (Waters, Milford, USA). The
299 samples were loaded into a trap column (C_{18}, pore size 100 Å, particle diameter of 5 µm and
300 an inner diameter of 180 µm, length 20 mm) and eluted with 0.1 % formic acid/acetonitrile
301 gradient (350 µL/min, linear gradient 2-5 % acetonitrile in 2 min, 5-60 % acetonitrile in
302 20 min) from an analytical column (C_{18}, pore size 130 Å, particle diameter of 1.7 µm and an
303 inner diameter of 75 µm, length 150 mm) at 40 °C and subjected to mass spectrometry. The
304 spectra were recorded in a mass range of 50 to 1800 m/z with a 0.5 s/scan in positive mode.
305 The following parameters were used for the NanoLockSpray source: capillary voltage of
306 1.5 kV; sampling cone voltage of 30 V; source temperature of 100 °C; desolvation
307 temperature of 150 °C; cone glass flow 50 L/h; desolvation gas flow of 550 L/h. Leucine
308 enkephalin was used as a lock mass analyte using the lock spray channel (lock spray
309 capillary voltage, 2.5 kV). Analysis of spectra was performed by MassLynx V4.1 SCN813
310 (Waters).

311 For protein identification, a non-redundant version of *E. coli* MG1655 protein database (NCBI
312 Bio Project accession PRJNA647163) with 4740 protein entries (plus the sequences of
313 trypsin and human keratin) and the ProteinLynxGlobalServer (PLGS) software V3.5.3
314 (Waters) with the following parameters were used: chromatographic peak width, automatic;

315 MS ToF resolution, automatic; lock mass window, 0.3 Da; low energy threshold, 50 counts.
316 Other parameters were as follows: peptide tolerance, automatic; fragment tolerance,
317 automatic; minimal fragment ion matches per peptide, 2; minimal fragment ion matches per
318 protein, 5; minimal peptide matches per protein, 2; maximum protein mass, 250 kDa; primary
319 digest reagent, trypsin; secondary digest reagent, none; missed cleavages, 1; fixed
320 modifications, carbamidomethyl C; variable modifications, deamination N and Q, oxidation M;
321 false positive rate, 4 %. The following parameters were considered for protein assignment:
322 Coverage of identified protein was > 10 %, at least 3 peptide ions and 5 product ions were
323 assigned, and theoretical pI and MW were consistent with the spot's position on the 2 D gel.

324 **RoGFP2 expression in bacteria.**

325 To measure the redox state in the cytoplasm of *E. coli* MG1655 and *B. subtilis* 168, cells
326 were transformed with the pCC_roGFP2 plasmid as described (Müller et al., 2017) and
327 pSG1729_roGFP2, respectively. pSG1729_roGFP2 cannot replicate in *B. subtilis*, but part of
328 it integrates into the *amyE* locus on the chromosome through a double-crossover event. To
329 create pSG1729_roGFP2, the EGFP insert from pSG1729 (Lewis and Marston, 1999) was
330 removed using KpnI and HindIII restriction enzymes. The gene sequence of roGFP2, codon-
331 optimized for *B. subtilis*, was amplified from pMX_roGFP2 (Thermo Fischer Scientific) by
332 PCR. Restriction sites for KpnI and HindIII were introduced using the primers JY001_for and
333 JY001_rev. Plasmid construction followed standard procedures and was performed in *E. coli*
334 DH5α. After successful plasmid construction, confirmed by sequencing, pSG1729_roGFP2
335 was transformed into *B. subtilis* 168 using standard protocols (Anagnostopoulos and
336 Spizizen, 1961), and selection for chromosomal insertion of the plasmid was performed on
337 LB plates containing 100 µg/mL spectinomycin. Double crossover of positive clones was
338 confirmed by the inability to hydrolyze starch on LB plates containing 0.5 % starch and
339 subsequent PCR amplification of the chromosomal insert and sequencing of the PCR
340 product.

341 For roGFP2 expression in *E. coli* MG1655, cells were grown in MOPS medium at 37 °C and
342 125 rpm. 200 µM of IPTG were used to induce protein expression at an OD_{600} of 0.4-0.6, and
343 roGFP2 was subsequently expressed for 16 h at 20 °C and 125 rpm in MOPS medium. After
344 expression, cells were harvested, washed in HEPES buffer (40 mM, pH 7.4), and adjusted to
345 an OD_{600} of 1.2.

346 For roGFP2 expression in *B. subtilis* 168, a single colony was inoculated in DSM medium
347 (Bacto nutrient broth 0.8 % (w/v), KCl 13.4 mM, $MgSO_4$ 1 mM, $Ca(NO_3)_2$ 1 mM, $MnCl_2$ 10 µM,
348 $FeSO_4$ 1 µM) containing 0.1 % xylose (w/v), and cells were grown for 16 h at 30 °C and

200 rpm. Cells were harvested, washed in BMM medium (Stulke et al., 1993), and incubated for 30 min at 25 °C and 800 rpm in a ThermoMixer (Eppendorf, Hamburg, Germany). The final OD_{600} was adjusted to 5. Cells were treated with 200 µM aldrithriol-2 (Sigma-Aldrich) (AT-2) as an oxidation control and 2 mM dithiothreitol (Sigma-Aldrich) as a reduction control. 0.5, 1, and 5 µM auranofin were used as treatment. As AT-2 and auranofin were dissolved in DMSO, an equivalent volume of DSMO was added to all samples. 1 mL of cell suspension was added to a 1500 µL Quartz Suprasil fluorescence cuvette (Hellma, Müllheim, Germany) with a stirring bar. Measurements were done at 25 °C in a JASCO FP-8500 fluorescence spectrometer equipped with the temperature-controlled sample holder 'EHC-813' at 25 °C for 60 min under continuous stirring. Measurement parameters in *E. coli* were as follows: 510 nm (Em), 350–500 nm (Ex), 5 nm slit width (Ex/Em), and medium sensitivity. After stabilization, respective treatments were added at the indicated final concentrations, and a time series of 61 additional spectra was recorded. Measurement parameters for *B. subtilis* were as follows: 520 nm (Em), 350–500 nm (Ex), 10 nm slit width (Ex/Em), and high sensitivity. After stabilization, respective treatments were added at the indicated final concentrations, and a time series of 61 additional spectra was recorded. The ratios of the fluorescence excitation intensities (405/488 nm) were used to calculate the probe's oxidation state. All values were normalized to fully oxidized (AT-2-treated) and fully reduced (DTT-treated) roGFP2 with the following equation [1]:

$$OxD = \frac{R - R_{red}}{\left(\frac{I_{488}ox}{I_{488}red}\right) * (R_{ox} - R) + (R - R_{red})}$$

R_{ox} is the 405/488 nm ratio of oxidized (AT-2 treated) and R_{red} of reduced (DTT-treated) cells expressing roGFP2, respectively. $I_{488}ox$ and $I_{488}red$ are the fluorescence intensities at 488 nm under oxidizing (i.e., AT-2) or reducing (i.e., DTT) conditions. R is the measured 405/488 nm ratio of the sample.

For calculation and normalization of the probe's oxidation degree at each time point, the means of all values recorded at all time points for R_{red}, R_{ox}, $I_{488}ox$, and $I_{488}red$ were used. Data was processed using Microsoft Excel software and GraphPad Prism version 10.1.0.

378 **RESULTS**

379 **Auranofin is antibacterial, but less effective against *E. coli* and other Gram-negative**
380 **species.**

381 Previous studies have shown that auranofin possesses potent bactericidal activity against
382 many Gram-positive bacteria but seems to be markedly less effective against pathogenic
383 Gram-negative species (Cassetta et al., 2014; Harbut et al., 2015; Hokai et al., 2014).
384 However, the reasons for the poor susceptibility of Gram-negative bacteria to auranofin are
385 not entirely clear. We analyzed the antimicrobial activity of auranofin against Gram-negative
386 and Gram-positive bacterial strains by minimal inhibitory concentration (MIC) assays. For this
387 purpose, we added various concentrations of auranofin to a defined number of bacterial cells
388 of *B. subtilis* 168, *S. aureus* DSM 20231/ATCC 43300, *P. aeruginosa* DSM 50071,
389 *A. baumanni* DSM 30007 and *E. coli* DSM 30083 and examined their growth after overnight
390 incubation. The MIC was defined as the lowest auranofin concentration, at which no visibly
391 perceptible bacterial growth was observed. In line with expectations, auranofin showed
392 potent growth inhibition against Gram-positive bacteria, with an MIC of 0.5 µg/mL for each
393 Gram-positive strain tested (Table 2). The MIC values determined for auranofin against *S.*
394 *aureus* and *B. subtilis* correlate with those reported in previous studies (Cassetta et al., 2014;
395 Harbut et al., 2015; Hokai et al., 2014). In contrast, auranofin exhibited poor antimicrobial
396 activity against Gram-negative bacteria, with MICs of 128 µg/mL, 32 µg/mL, and 512 µg/mL
397 against *E. coli*, *A. baumannii,* and *P. aeruginosa*, respectively, which agrees with previous
398 reports (Harbut et al., 2015; Thangamani et al., 2016).

399

400 **Table 2: MICs of Auranofin against various Gram-negative and Gram-positive bacterial species.**
401

Strain	MIC, µg/mL
Gram-negative bacteria	
E. coli DSM 30083	128
A. baumannii DSM 30007	32
P. aeruginosa DSM 50071	512
Gram-positive bacteria	
B. subtilis 168	0.5
S. aureus DSM 20231	0.5
S. aureus ATCC 43300 (MRSA)	0.5

402

403 **Auranofin causes upregulation of proteins involved in central metabolism and the**
404 **defense against oxidative stress in *E. coli*.**

405 To understand if auranofin exposure leads to a markedly different cellular response in Gram-
406 negative bacteria, we performed proteomics experiments in *E. coli*. We compared our results
407 to our results previously obtained for *B. subtilis* (Senges et al., 2020). In our experiments, we
408 treated an exponentially growing culture of *E. coli* MG1655 with a sublethal concentration of
409 120 µg/mL auranofin. This concentration was found to partially inhibit bacterial growth by
410 26.27 ± 4.14 % (Fig. 1a). Upon exposure to auranofin for 10 min, the cells were pulse-
411 labeled for 5 minutes with L-[^{35}S]-methionine, which was incorporated into newly synthesized
412 proteins. Quantification of total L-[^{35}S]-methionine incorporation revealed no significant
413 difference between the control and the auranofin-treated culture, suggesting that auranofin
414 does not directly inhibit protein synthesis (Fig. 1b).

415 Newly synthesized proteins were quantified by densitometry of radioactive spots after two-
416 dimensional PAGE. Auranofin-induced changes in protein synthesis patterns were visualized
417 by overlaying the gel images of the L-[^{35}S]-methionine-labeled proteins under control
418 conditions (green) and after treatment with auranofin (red). Protein spots synthesized only
419 under control conditions appear in green; protein spots that were synthesized only upon
420 auranofin treatment appear in red, whereas protein spots synthesized under both conditions
421 appear yellow. Out of the three independent experiments, a representative dual-channel
422 image produced from autoradiographs of 2D gels obtained for control and auranofin-treated
423 cells is shown in Fig. 1c. Auranofin treatment caused a more than two-fold increase in
424 relative synthesis rates of 30 protein spots (indicated by arrows). From non-radioactive gels,
425 proteins could be identified by mass spectrometry in 20 of those spots (Fig. 1c, Tables 3 and
426 S2).

427 Most identified marker proteins upregulated in response to auranofin treatment are
428 associated with a specific response to oxidative stress and/or involved in cellular processes
429 such as ROS detoxification, central metabolism, amino acid biosynthesis, and metal
430 homeostasis.

431 Many of the upregulated proteins are enzymes of the central metabolic network, such as
432 GpmM (phosphoglycerate mutase), PykF (pyruvate kinase I), Lpd (lipoamide
433 dehydrogenase), and the alpha subunit of the ATP synthase F_1 complex of the electron
434 transport chain AtpA. Auranofin treatment was also found to increase the synthesis of the
435 enzyme dihydroorotase (PyrC), which functions in the pathway for the biosynthesis of
436 pyrimidine nucleotides. Some other induced proteins, such as AhpF and AhpC, which are
437 components of the alkyl hydroperoxide reductase, and Gor (glutathione oxidoreductase),

438 belong to the OxyR regulon and are involved in the protection against peroxide and in
439 maintaining redox balance (Storz et al., 1990; Storz and Tartaglia, 1992). Gor is responsible
440 for recycling the glutathione pool NADPH-dependently. NADPH is thought to be delivered by
441 the pentose pathway, of which RpiA was upregulated. A similar observation was made in our
442 laboratory when *E. coli* cells were subjected to diamide or the antimicrobial compound allicin,
443 both known to induce disulfide stress (Müller et al., 2013, 2016): here, central metabolic
444 enzymes and OxyR-dependent proteins were upregulated, as well. Additionally, auranofin
445 treatment led to the upregulation of a sulfur assimilation enzyme (CysN) for the biosynthesis
446 of sulfur-containing amino acids and the oxidative stress-protective multicopper oxidase
447 CueO.

448 To test if one of these upregulated proteins is directly involved in *E. coli*'s tolerance against
449 auranofin, we tested, if selected single mutants from the KEIO collection lacking these
450 proteins were more susceptible to auranofin in an MIC assay. The mutants lacking GpmM,
451 Pgk, Lpd, and PyrC did not grow in MOPS medium. None of the proteins missing in the
452 selected mutants that did grow, impacted the MIC when absent, except for NemA (Table 3).
453 The Δ*nemA* strain was found to be slightly more resistant to auranofin treatment and had an
454 MIC of 256 µg/mL (WT being 128 µg/mL).

455 Overall, the proteomic results indicate that auranofin-treated cells suffer systemic oxidative
456 stress. This could lead to the direct inactivation of essential thiol-containing enzymes, e.g., in
457 the central metabolism, and a depletion of free cysteine levels or, more generally, thiol levels.
458 We made a similar observation in *B. subtilis* (Senges et al., 2020), and based on our
459 proteome data, we could not differentiate between the mode of action of auranofin in Gram-
460 positive and Gram-negative bacteria.

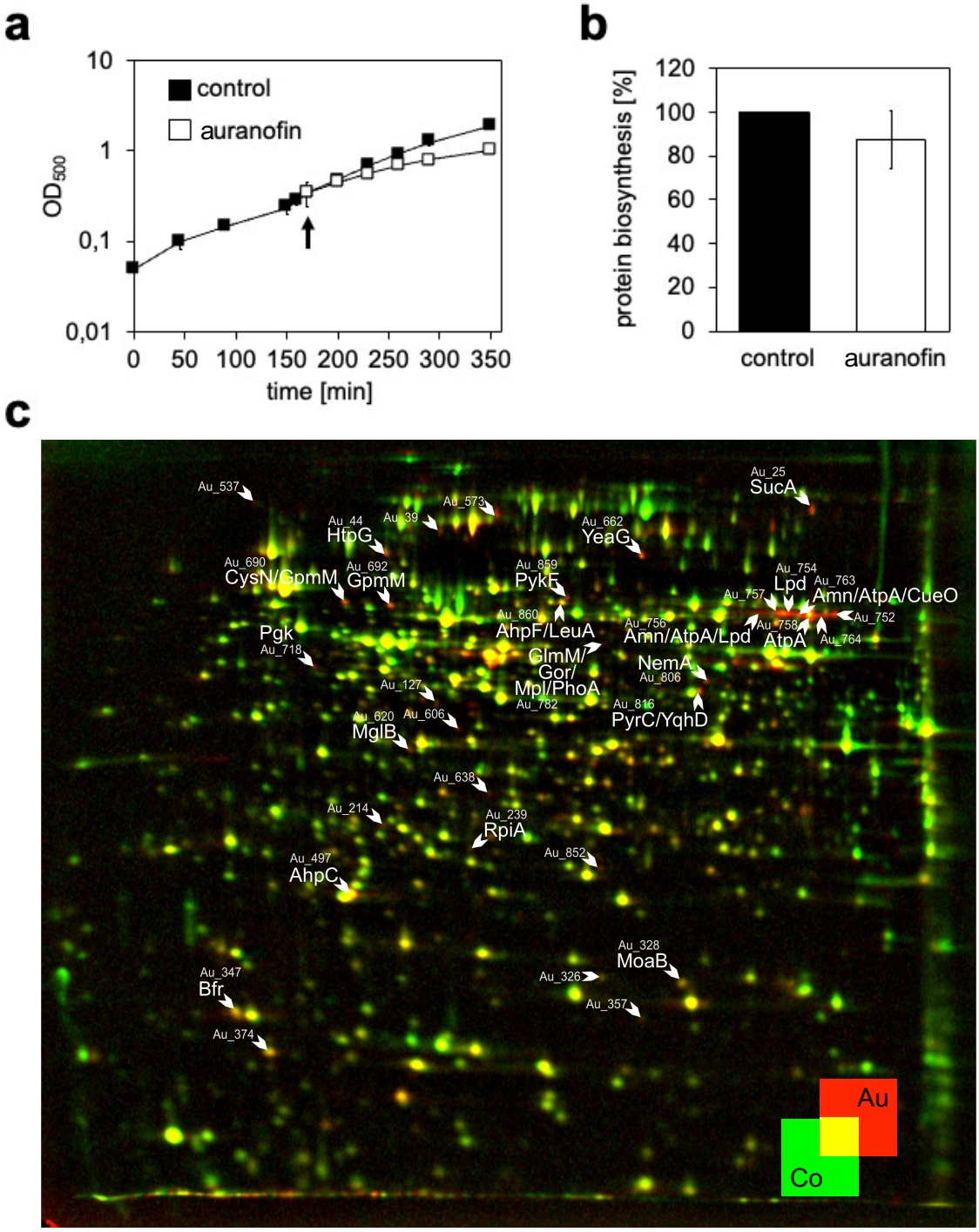

Figure 1: Proteomic response of *E. coli* MG1655 stressed with 120 µg/mL Auranofin. (a) Growth curves of *E. coli* MG1655 grown in MOPS media at 37 °C and 200 rpm without auranofin (■) and after the addition of 120 µg/mL auranofin (□). An arrow indicates the timepoint of auranofin addition. **(b)** Incorporation of L-[^{35}S]-methionine during a 5 min pulse starting 10 min after treatment with 120 µg/mL auranofin. **(c)** 2D-PAGE analysis of the pulse-labeled proteomics response profile of *E. coli* MG1655 treated with 120 µg/mL auranofin. False-color overlay of treated and untreated radioactive gels shows proteins synthesized after pulse labeling for 5 min after treatment with auranofin (red, Au) or in the untreated control (green, Co). Upregulated proteins with a regulation factor ≥ 2 were considered marker proteins and were labeled by arrows and the Spot ID Au_X. Marker proteins identified by mass spectrometry are additionally labeled with the protein's name. For Spot ID, identified proteins, and functions, see Table 3 and Supplemental Table S2. **(a, c)** Representative example from 3 **(a)** or 2 **(c)** biological replicates. **(b)** Average and standard deviation of 3 biological replicates.

476 **Table 3: Identified marker proteins of auranofin-treated *E. coli* MG1655.** Protein functions and
477 accession number (EcoCyc ID) were taken from the EcoCyc database (Keseler et al., 2017). Regulation
478 factor (Reg. factor) is the average of 2 biological replicates. The MIC of the corresponding deletion
479 mutant is shown (n=3). Deletion mutants not viable in minimal medium are marked by n. v., MIC not
480 determined is marked by n. d.
481

Spot ID	Reg. factor	Protein (EcoCyc ID)	Function	MIC µg/mL
497	2.3	**AhpC** (EG11384)	alkyl hydroperoxide reductase, AhpC component	128
860	3.6	**AhpF** (EG11385)	alkyl hydroperoxide reductase, AhpF component	128
		LeuA (EG11226)	2-isopropylmalate synthase	n.d.
763	4.6	**Amn** (EG10039)	AMP nucleosidase	128
		AtpA (EG10098)	ATP synthase F1 complex subunit α	128
		CueO (EG12318)	multicopper oxidase CueO	128
756	4.0	**Amn** (EG10039)	AMP nucleosidase	128
		AtpA (EG10098)	ATP synthase F1 complex subunit α	128
		Lpd (EG10543)	lipoamide dehydrogenase	n.v.
758	15.0	**AtpA** (EG10098)	ATP synthase F1 complex subunit α	128
347	3.2	**Bfr** (EG10113)	bacterioferritin	128
690	2.1	**CysN** (EG10194)	sulfate adenylyltransferase subunit 1	128
		GpmM (EG12296)	2,3-bisphosphoglycerate-independent phosphoglycerate mutase	n.v.
782	4.0	**GlmM** (EG11553)	phosphoglucosamine mutase	n.d.
		Gor (EG10412)	glutathione reductase	128
		Mpl (EG12440)	UDP-N-acetylmuramate-L-alanyl-γ-D-glutamyl-meso-2,6-diaminoheptanedioate ligase	n.d.
		PhoA (EG10727)	alkaline phosphatase	n.d.
692	2.6	**GpmM** (EG12296)	2,3-bisphosphoglycerate-independent phosphoglycerate mutase	n.v
44	4.1	**HtpG** (EG10461)	chaperone protein HtpG	n.d.
754	7.2	**Lpd** (EG10543)	lipoamide dehydrogenase	n.v.
620	2.7	**MglB** (EG10593)	D-galactose/methyl-galactoside ABC transporter periplasmic binding protein	128
328	2.4	**MoaB** (EG11596)	protein MoaB	128
806	3.9	**NemA** (G6890)	N-ethylmaleimide reductase	256
718	6.1	**Pgk** (EG10703)	phosphoglycerate kinase	n.v.
859	3.6	**PykF** (EG10804)	pyruvate kinase 1	128
816	3.0	**PyrC** (EG10806)	dihydroorotase	n.v.
		YqhD (G7564)	NADPH-dependent aldehyde reductase YqhD	n.d.
239	2.0	**RpiA** (EG11443)	ribose-5-phosphate isomerase A	n.d.
25	3.2	**SucA** (EG10979)	2-oxoglutarate decarboxylase, thiamine-requiring	128
662	3.9	**YeaG** (G6969)	protein kinase YeaG	128

482 **The higher resistance against auranofin can be partially explained by more effective**
483 **efflux systems in Gram-negative bacteria.**

484 Efflux pumps are critical players in antimicrobial resistance in Gram-negative bacteria. These
485 pumps actively transport a variety of substrates, including antibiotics and heavy metals, out
486 of the bacterial cell, thereby reducing the intracellular concentration of these compounds and
487 conferring resistance to the cell. The outer membrane protein TolC, part of the small
488 multidrug resistance (SMR) protein family, is a significant component involved in the export
489 of various cytotoxic substances. Studies have shown that mutations in the TolC protein
490 resulted in sensitivity to different antibiotics, such as vancomycin, erythromycin, and
491 novobiocin (Augustus et al., 2004), and an increased susceptibility to metal ions (Munita and
492 Arias, 2016).

493 We found that cellular susceptibility to auranofin was increased two-fold when we tested the
494 MIC of an *E. coli* Δ*tolC* strain (Table 4). The MICs of *B. subtilis* and *S. aureus* were 0.5 µg/ml,
495 i.e., still more than two orders of magnitude lower than that of the TolC-deficient *E. coli* strain.
496 This suggests that TolC does play a role in the efflux of auranofin from the bacterial cell,
497 albeit not to an extent that would fully explain the overall higher resistance of Gram-negative
498 bacteria.

499 **Table 4: MICs of Auranofin against *E. coli* BW25113 and *E. coli* BW25113 Δ*tolC*.**
500

Strain	MIC, µg/mL
E. coli BW25113 (WT)	128
E. coli JW5503 (BW25113 Δ*tolC*)	64

501

502 **Auranofin inhibits TrxB from both *E. coli* and *B. subtilis* to a similar extent.**

503 Evidence suggests that auranofin primarily exerts its effect by targeting bacterial thiol-redox
504 homeostasis by inhibiting thioredoxin reductase (TrxB) (Harbut et al., 2015; Hokai et al.,
505 2014). Since TrxB is responsible for reducing oxidized thioredoxin (TrxA) and, thus, for
506 maintaining a reducing intracellular environment, loss of TrxB activity can lead to severe
507 oxidative stress in an organism with no alternative antioxidant system, such as the
508 glutathione/glutaredoxin system.

509 While auranofin has been found to effectively inhibit TrxB of *S. aureus*, *M. tuberculosis,* and
510 other Gram-positive bacterial species (Harbut et al., 2015; Owings et al., 2016), less is
511 known about its inhibitory potency towards TrxB of Gram-negative bacteria. Hence, one
512 possible explanation for auranofin's limited antibacterial activity against Gram-negative

513 bacteria might be that auranofin is a less effective inhibitor of TrxB in these organisms when
514 compared to Gram-positive bacteria. To explore this hypothesis, we tested auranofin's
515 effectiveness in a biochemical assay with TrxB from Gram-negative and Gram-positive
516 bacteria, with *E. coli* and *B. subtilis* as representative organisms, respectively.

517 The activity of purified TrxB from *E. coli* and *B. subtilis* (from now on referred to as "*ec*TrxB"
518 and "*bs*TrxB", respectively) was then determined in the presence of NADPH, and various
519 auranofin concentrations by performing a 5,5'-dithiobis(2-nitrobenzoic) acid (DTNB) reduction
520 assay (Arnér and Holmgren, 2005). The NADPH-dependent TrxB reduces DTNB in this
521 assay, yielding the detectable 5-thio-2-nitrobenzoic acid (TNB). The amount of liberated TNB
522 can be quantified spectrophotometrically by measuring its absorbance at 412 nm.

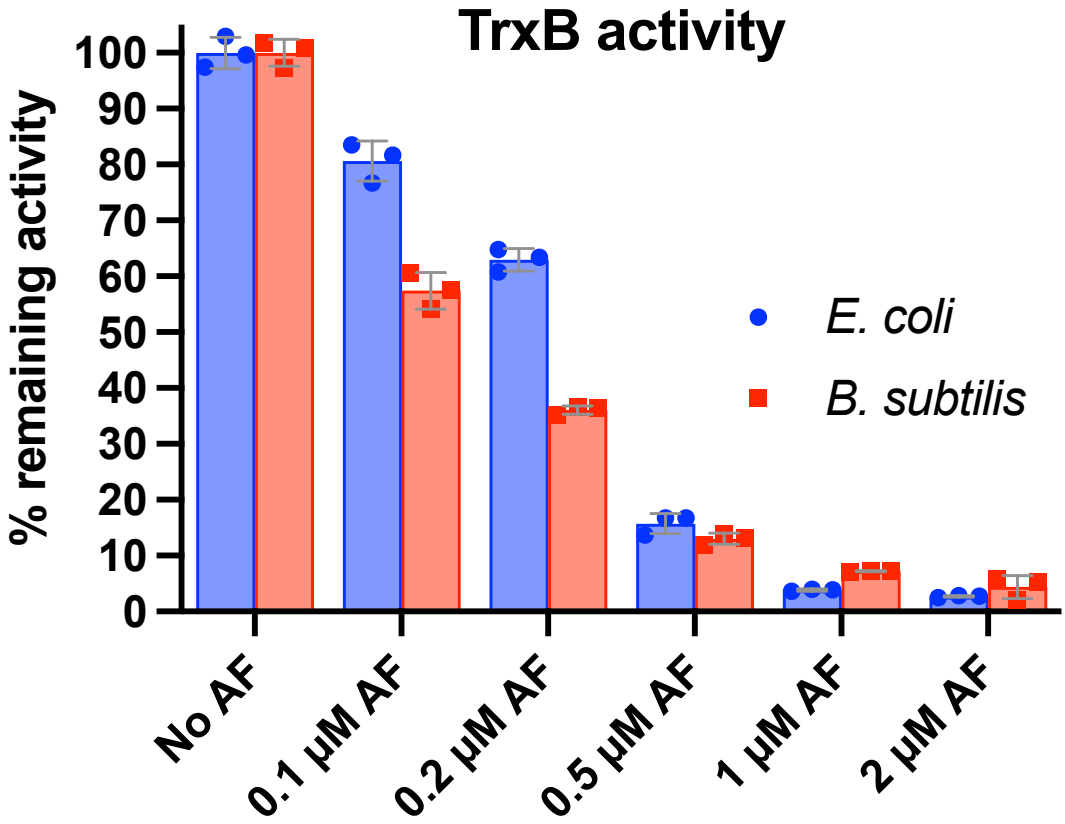

523
524

525 **Figure 2: Auranofin inhibits *E. coli* (*ec*TrxB) and *B. subtilis* TrxR (*bs*TrxB) in a dose-dependent**
526 **manner.** Purified *ec*TrxB and *bs*TrxB (1 µM) were preincubated with 200 µM NADPH in the absence (0
527 µM auranofin) or presence of various auranofin concentrations (0.1 to 2 µM) for 5 min. The addition of
528 2 mM DTNB initiated the reaction. Reaction progress was monitored by measuring the absorbance of
529 the liberated TNB chromophore at 412 nm over time. Experiments were performed in triplicates. Mean
530 (bars), individual values (dots) and SD are shown (error bars).
531

532 When auranofin was preincubated with 1 µM *ec*TrxB or *bs*TrxB, auranofin inhibited both
533 enzymes dose-dependently. The activity measurements showed potent and nearly complete
534 inhibition of *ec*TrxB and *bs*TrxB already at equimolarity (1 µM auranofin, corresponding to ~
535 0.68 µg/mL) (Fig. 2). While the auranofin concentration required to fully inhibit TrxB agreed
536 well with the previously determined MIC against *B. subtilis* (Table 1), it was far below the
537 level required to exhibit cytotoxicity towards *E. coli*. This observation strongly suggests that
538 the lower antimicrobial activity of auranofin against *E. coli* is not due to a lower affinity of
539 auranofin for *ec*TrxB.

540 **Trx reductase is not the only target of Auranofin in Gram-negative bacteria.**

541 Based on the results of our biochemical activity assays, we suspected that TrxB may not be
542 the only target of auranofin in *E. coli*. We speculated that other redox pathway components
543 might also be involved in the mechanism of action of auranofin. To test our hypothesis, we
544 analyzed auranofin's antimicrobial activity against additional mutants of the KEIO collection
545 (Baba et al., 2006). The mutants we chose lack components of the Trx antioxidant system,
546 i.e., the redox protein thioredoxin TrxA (Δ*trxA*; *E. coli* JW5156) or TrxB (Δ*trxB*; *E. coli*
547 JW0871) itself, respectively (Fig. 3). Growth of the selected *E. coli* strains in the absence of
548 auranofin was monitored until an OD_{600} of 0.5 was reached. *E. coli* mutant strains without a
549 functional Trx system showed a comparable or only slightly lower growth rate than the wild
550 type, excluding the possibility that potential differences in the susceptibility of the different
551 strains to auranofin are solely due to a generally impaired growth of the deletion mutants
552 (Fig. 3a). The cultures were then used to inoculate medium containing different amounts of
553 auranofin for an MIC assay. After overnight incubation, cultures were analyzed for growth. *E.*
554 *coli* deficient in TrxA or TrxB showed a four-fold increased sensitivity to auranofin compared
555 to wild-type *E. coli*, with MICs of 32 µg/mL (Δ*trxA* and Δ*trxB*) in contrast to 128 µg/mL (WT)
556 (Fig. 3b, c). The increased susceptibility of *E. coli* mutants lacking a functional Trx system,
557 especially the suspected target TrxB, indicates that auranofin leads to global oxidative stress
558 not only through TrxB inhibition but also in a direct manner or through inhibition of other thiol-
559 disulfide oxidoreductase systems.

560 **The glutathione reductase confers no resistance to auranofin, while the glutathione**
561 **pool by itself has a substantial effect on the MIC.**

562 Although auranofin showed a generally higher efficacy against *E. coli* strains deficient in the
563 functional Trx system, the MIC values were still markedly higher than those observed with
564 Gram-positive bacteria. In contrast to most Gram-negative bacteria, many Gram-positive
565 species lack glutathione. Glutathione by itself is considered an antioxidant, and with the small

566 redox protein glutaredoxin, it can compensate for the loss of a functional Trx system (Gon et
567 al., 2006). In Gram-positive organisms, on the other hand, the Trx system is essential (Lu
568 and Holmgren 2014; Uziel et al. 2004; Scharf et al. 1998). Hence, the additional
569 glutathione/glutaredoxin system in Gram-negative bacteria could be a reason for auranofin's
570 low potency against *E. coli* and other Gram-negative species. However, we already knew
571 from our MIC tests performed in mutants deficient in proteins upregulated in our proteomics
572 experiments that a Δ*gor* mutation did not affect the MIC. Thus, we argued that the absence
573 of a functional glutaredoxin-system does not play a role. We then tested if glutathione, the
574 tripeptide itself, could play an important role instead. Both, deletion of glutathione
575 oxidoreductase (Δ*gor*) and γ-glutamate-cysteine-ligase (Δ*gshA*), the enzyme catalyzing the
576 first step of glutathione biosynthesis, did not affect *E. coli*'s growth in the absence of
577 auranofin (Fig. 3a). But auranofin's activity against *E. coli* Δ*gshA* was markedly higher than
578 against the WT or Δ*gor*, which both had the same MIC. The MIC of Δ*gshA* decreased to 8
579 µg/mL (Fig. 3b, c), closer to the MIC observed in Gram-positive bacteria. The increase in *E.*
580 *coli's* sensitivity to auranofin upon depletion of the intracellular glutathione pool suggests that
581 this monothiol, typically present at concentrations in the millimolar range, confers substantial
582 protection against oxidative stress induced by auranofin.

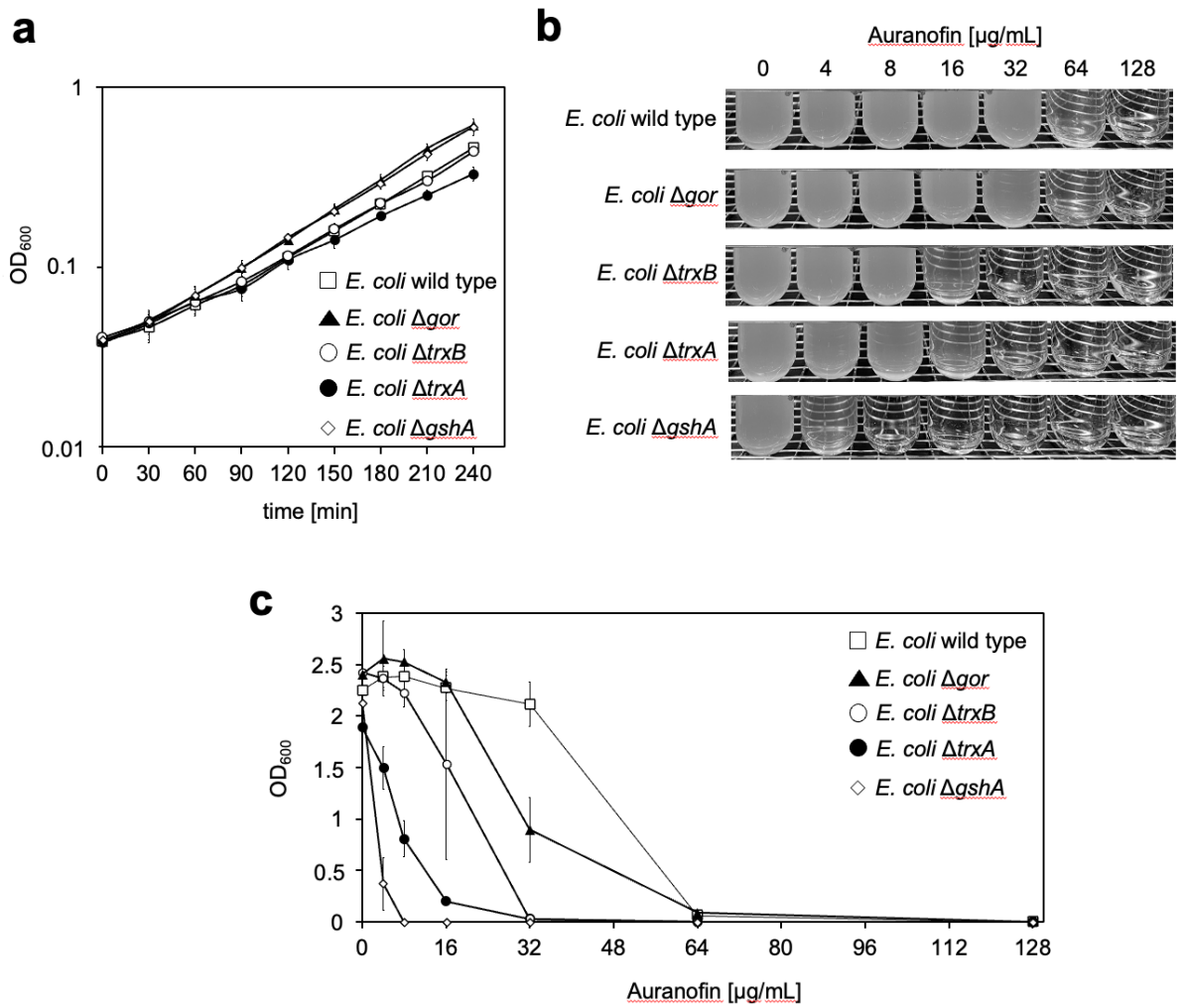

Figure 3: Loss of a functional Trx system and depletion of the glutathione pool increase *E. coli's* susceptibility to auranofin. (a) Growth curves of *E. coli* BW25113 (wild type) and single-gene knockout mutants of the KEIO collection (Baba et al., 2006) lacking a functional *gor* (Δ*gor*; *E. coli* JW3467), *gshA* (Δ*gshA*; *E. coli* JW2663), *trxB* (Δ*trxB*; *E. coli* JW0871), or *trxA* gene (Δ*trxA*; *E. coli* JW5156), respectively, in the absence of auranofin. **(b, c)** MICs of auranofin against *E. coli* wild type and the various mutant strains. Cells were grown in MOPS minimal medium until an OD_{600} of 0.5 was reached. The various cultures were then used to inoculate MOPS minimal medium containing the indicated amounts of auranofin with 10^5 cells. After overnight incubation, bacterial growth was analyzed **(b)** visually and **(c)** photometrically by measuring the OD_{600} of the cultures. **(b)** A representative MIC assay is shown. **(c)** Means and standard deviations of three independent experiments are shown.

Auranofin leads to thiol oxidation in the cytosol.

We then wanted to measure the intracellular thiol redox state in auronofin-treated bacteria *in situ*. roGFP2 is a genetically engineered variant of GFP containing two cysteines, which form a disulfide bridge upon oxidation, thereby changing the protein's fluorescent properties. This can be used to determine the oxidation degree of roGFP2 (Aller et al., 2013), independent of the probe's concentration (Dooley et al., 2004; Meyer and Dick, 2010; Müller et al., 2017). Because we assumed that auranofin interferes not only with TrxB but with the oxidation state

603 of thiols in general, we used roGFP2 as a tool to monitor the redox state of cysteines in
604 cellular proteins. We expressed roGFP2 in the cytoplasm of both *B. subtilis* and *E. coli*. We
605 then determined the oxidation degree of roGFP2 inside the cells. The oxidant AT-2 was used
606 to fully oxidize, and the reductant DTT to fully reduce roGFP2 within cells, setting the fully
607 reduced and fully oxidized baselines of our probe within the bacterial cell. In both strains, the
608 probe is more or less fully reduced in the cytosol of untreated cells. Using a concentration of
609 5 µM auranofin, the degree of oxidation of roGFP2 increases by 40 % after 60 min of
610 treatment in *E. coli* (Fig. 4b), whereas it increases by up to 90 % in less than 1 min in
611 *B. subtilis* (Fig. 4a). Lower concentrations of 1 µM or 500 nM auranofin still increased the
612 oxidation state of roGFP2 in *B. subtilis* to around 80 % within 5 min of treatment, while in
613 *E. coli* an oxidation state of only 10 to 20 % was reached after 60 min. The subsequenmt
614 addition of 2 mM DTT to the cells led to an immediate decrease in probe oxidation in all
615 cases, demonstrating that, in principle, the change in cellular oxidation imposed by auranofin
616 is reversible by thiol reductants in both organisms.

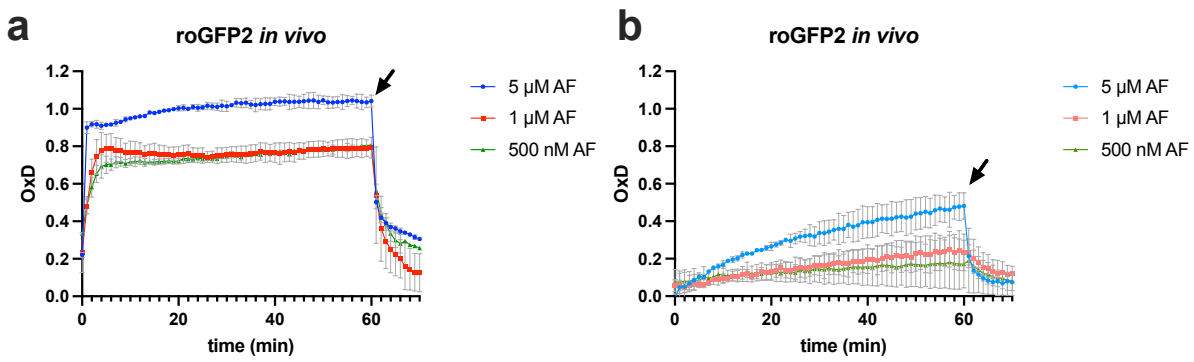

617

618 **Figure 4: Auranofin exposure leads to roGFP2 oxidation *in vivo*.** To evaluate the effects of auranofin
619 on protein thiols in bacteria *in situ*, *B. subtilis* **(a)** and *E. coli* **(b)** expressing roGFP2 were treated with
620 0.5, 1, or 5 µM auranofin. Aldrithiol-2 and dithiothreitol were used to fully oxidize and fully reduce the
621 probe within cells, respectively, and these baselines (not shown) were used to calculate the oxidation
622 degree (OxD) of roGFP2. OxD normalizes the ratiometrically determined redox state and accounts for
623 differences in probe synthesis and measurement settings. roGFP2 fluorescence was measured at an
624 emission wavelength of 510 nm, and the excitation wavelength was scanned from 350–500 nm. roGFP2
625 oxidation was monitored for 60 minutes after adding auranofin, and then DTT was added at a
626 concentration of 2 mM (indicated by an arrow).

627 **DISCUSSION**

628 The gold(I) compound auranofin, an FDA-approved antirheumatic drug, has recently been
629 found to possess antimicrobial activity and, thus, is a promising candidate for drug
630 repurposing for treating multidrug-resistant infections. Although auranofin shows high activity
631 against a considerable range of Gram-positive bacteria, it seems less effective against
632 Gram-negative species (Harbut et al., 2015; Owings et al., 2016). In the present study, we
633 aimed to understand the underlying mechanism of the difference in susceptibility of Gram-
634 negative and Gram-positive bacteria to auranofin.

635 We thus tested auranofin's ability to inhibit the growth of different Gram-positive and Gram-
636 negative species. Growth of Gram-positive strains was prevented by an auranofin
637 concentration as low as 0.5 µg/mL. These results agree with previously reported MICs
638 against *B. subtilis* PY79*, M. tuberculosis,* and several methicillin-resistant *S. aureus* (MRSA)
639 strains (Harbut et al., 2015; Hokai et al., 2014). As expected, a substantial difference in the
640 effective concentration of auranofin was found for the Gram-negative species
641 *A. baumannii* DSM 30007, *E. coli* DSM 30083, and *P. aeruginosa* DSM 50071 with MIC
642 values of 32, 128, and 512 µg/mL, respectively.

643 Proteomic profiling of auranofin-stressed *E. coli* revealed that its cellular response is similar
644 to the response of *B. subtilis*. *B. subtilis* was found to counteract auranofin stress by
645 specifically upregulating enzymes that detoxify ROS, such as the catalase KatA, or replenish
646 the cysteine pool, such as YrhB (Senges et al., 2020). Similarly, in *E. coli*, proteins belonging
647 to the OxyR regulon, such as AhpC and AhpF, the two components of *E. coli*'s alkyl
648 hydroperoxide reductase and glutathione oxidoreductase Gor, were upregulated significantly.
649 The transcription factor OxyR regulates the expression of antioxidant genes in response to
650 oxidative stress, particularly elevated levels of hydrogen peroxide (Storz et al., 1990; Storz
651 and Tartaglia, 1992). We showed previously that OxyR-dependent genes are also
652 upregulated in response to the oxidant diamide and the antimicrobial compound allicin, both
653 of which were found to induce disulfide stress in *E. coli* (Müller et al., 2013, 2016). We then
654 tested the susceptibility of mutants devoid of proteins upregulated in our proteomic
655 experiments to auranofin. None of the mutants tested showed a lower MIC and, thus, higher
656 susceptibility to auranofin, suggesting that these proteins are not the reason for *E. coli*'s high
657 tolerance for auranofin.

658 Previous studies on auranofin as an antimicrobial drug suggested that, as in mammals, the
659 flavoenzyme thioredoxin reductase (TrxB) is a primary target in bacteria (Harbut et al., 2015).
660 Our studies showed that auranofin inhibits mammalian TrxR with a K_i of only 4 nM (Gromer
661 et al. 1998). Along this line, auranofin has been shown to effectively inhibit bacterial TrxB

662 from numerous Gram-positive pathogens, including *M. tuberculosis* and *S. aureus* (Fuchs et
663 al., 2016; Harbut et al., 2015). However, it should be noted that bacterial TrxB is structurally
664 significantly different from mammalian TrxR and does not contain selenocysteine (Lu and
665 Holmgren, 2014). Selenocysteine is thought to play a major role in the inhibition of
666 mammalian TrxR by auranofin: Several lines of evidence suggest that selenocysteine is
667 either the direct binding site of auranofin or is essential for releasing the gold atom from its
668 ligands, given that the affinity of selenium for gold and its nucleophilic power are greater than
669 those of sulfur (Angelucci et al., 2009; Arscott et al., 1997; Dos Santos, 2014; Rigobello et
670 al., 2004, 2005). Additionally, TrxBs from Gram-positive and Gram-negative bacteria are
671 structurally much more similar to each other than to mammalian TrxR. Bacterial TrxB has
672 only a low degree of sequence homology (<30 %) to human TrxR (Arscott et al., 1997).

673 Nevertheless, to uncover potential differences in TrxB inhibition in Gram-negative and Gram-
674 positive bacteria, which could explain the different susceptibilities of the species, we
675 biochemically tested the inhibition of TrxB from *E. coli* (*ec*TrxB) and *B. subtilis* (*bs*TrxB) by
676 auranofin. We found that inhibition of both *ec*TrxB and *bs*TrxB by auranofin is dose-
677 dependent, and in both cases, an equimolar amount is enough to inhibit their activity entirely.
678 These observations suggest that inhibition of bacterial TrxB by auranofin could be
679 irreversible. In any case, no significant difference in susceptibility could be observed between
680 TrxB from Gram-positive and Gram-negative species in our assay. This shows that, at a
681 target level, both Gram-positive and Gram-negative species are equally susceptible.

682 To test other properties that could make Gram-negative bacteria more resistant to auranofin,
683 we examined an *E. coli* strain lacking TolC. This efflux pump removes antibiotics and metals
684 from the cell (Koronakis, 2003). We found that the lack of TolC decreased auranofin's
685 resistance only by a factor of two, not fully explaining Gram-negative organisms' substantially
686 higher resistance than Gram-positive bacteria.

687 Unlike most Gram-negative bacteria, many Gram-positive bacteria do not possess the low
688 molecular weight thiol glutathione and the glutaredoxin system. Hence, TrxB and its
689 substrate thioredoxin (TrxA) are considered the key mediators of redox homeostasis in these
690 organisms (Lu and Holmgren, 2014), and the Trx system is essential for *B. subtilis* and *S.*
691 *aureus*' survival at normal growth conditions and under oxidative stress (Scharf et al., 1998;
692 Uziel et al., 2004). Conversely, *E. coli* strains deficient in TrxB or TrxA did show only
693 moderately higher susceptibility towards auranofin. These findings, too, suggest that TrxB
694 may not be the sole target of auranofin in *E. coli*. Following up on the idea that glutathione
695 and the associated glutaredoxins could compensate for the loss of TrxB in *E. coli*, as
696 suggested by Harbut et al. (Harbut et al., 2015), we revisited auranofin's activity against an

697 *E. coli* mutant devoid of the glutathione reductase (Gor). As there was no difference in the
698 susceptibility to auranofin, in line with findings from Thangamani et al. (Thangamani et al.,
699 2016), we concluded that the glutaredoxin system as a backup for thioredoxin is not the main
700 reason for *E. coli*'s relative resistance to auranofin. However, the loss of the major
701 intracellular low molecular weight thiol glutathione itself led to a substantial increase in
702 sensitivity to auranofin. Therefore, several possible factors for the high tolerance of Gram-
703 negative bacteria towards auranofin must exist. First, Gram-negative bacteria possess more
704 effective mechanisms to avoid auranofin stress, i.e., the presence of efflux pumps, potentially
705 in combination with the presence of an outer membrane. Second, the presence of
706 glutathione was, in our experiments, the most effective contributor to auranofin resistance in
707 *E. coli*. Glutathione's high concentration of up to 10 mM in the cell could make it a potent
708 buffer against auranofin, depleting the gold compounds' ability to react with protein thiols.
709 These findings corroborate that auranofin induces disulfide stress not only through TrxB
710 inactivation but potentially through direct thiol modification in proteins and reaction with low
711 molecular weight thiols in general.

712 The cysteine-containing redox probe roGFP2, synthesized in the cytosol of bacterial cells,
713 revealed that auranofin indeed directly affected protein oxidation. A high oxidation degree
714 was reached within minutes in Gram-positive bacteria. This quick oxidation is not observed in
715 Gram-negative bacteria, presumably due to the existence of efflux pumps in combination
716 with the presence of high concentrations of glutathione.

717 In clinical trials with auranofin, plasma concentrations of auranofin ranging between 0.8 and
718 1.5 µg/mL were reached (Capparelli *et al.*, 2017). While this therapeutically achievable
719 auranofin concentration is sufficient to inhibit the growth of most Gram-positive pathogens, it
720 is 20 to 340 times lower than the auranofin concentration necessary to prevent the growth of
721 the tested Gram-negative strains, rendering auranofin virtually ineffective against these
722 organisms in a clinical setting. Its limited activity against Gram-negative bacteria currently
723 prevents its systemic clinical use as an antibiotic in treating infections with Gram-negative
724 pathogens. The results presented here strongly suggest that, while auranofin's mechanism of
725 action against *E. coli* does not substantially differ from that against *B. subtilis per se*, other
726 factors unique to Gram-negative bacteria are attenuating auranofin's antimicrobial
727 effectiveness. Thus, potential drugs based on auranofin's mechanism of action need to
728 account for those factors, particularly the presence of high cellular concentrations of
729 glutathione.

730 Our results indicate that the mode of action of auranofin in bacteria is a combination of the
731 inactivation of thiol-containing enzymes, a decrease of reduced Trx levels through TrxB

732 inactivation, and the induction of systemic oxidative stress. While most clinically used
733 antibiotics act on a single target, this broad-range effect of auranofin could prevent the
734 evolution of specific resistance mechanisms, and indeed several others reported that
735 spontaneous auranofin-resistant mutants cannot be generated (Harbut et al., 2015;
736 Thangamani et al., 2016; Elkashif and Seleem, 2020). This should make the development of
737 other gold-containing drugs, effective in Gram-negative bacteria, and based on auranofin's
738 mode of action a worthwhile endeavor.

AUTHOR CONTRIBUTIONS

J.E.B. and L.I.L. conceived and coordinated the study. A.U., A.M.I., M.V., and N.L. purified all proteins. M.F. and K.B. provided materials and developed protocols for the biochemical activity and inhibition assays. M.V-H. performed the experiments shown in Fig. 1. L.Q.B. performed the experiments shown in Fig. 2. A.M.I., M.V., and L.Q.B. performed the experiments shown in Fig. 3. L.Q.B and J. Y. performed the experiments shown in Fig. 4. A.U., L.Q.B., M.V., M.V-H., and L.I.L contributed to the analysis and interpretation of the results. A.U., L.Q.B. and L.I.L. wrote the manuscript. All authors approved the final version of the manuscript.

ACKNOWLEDGMENTS

L.I.L. and J.E.B. acknowledge funding from the German Research Foundation (DFG) through Research Training Group 2341 “Microbial Substrate Conversion (MiCon)”.

L.I.L. received additional funding through the InnovationsFoRUM Host-Microbe-Interaction IF-018N-22-TP8, and J.E.B. gratefully acknowledges funding from the German federal state of North Rhine-Westphalia for the mass spectrometer (Forschungsgrossgeräte der Länder).

We gratefully acknowledge the excellent support of the technical staff at RUBION, Ruhr University Bochum.

REFERENCES

Aguinagalde, L., Díez-Martínez, R., Yuste, J., Royo, I., Gil, C., Lasa, Í., Martín-Fontecha, M., Marín-Ramos, N. I., Ardanuy, C., Liñares, J., García, P., García, E., and Sánchez-Puelles, J. M. (2015). Auranofin efficacy against MDR *Streptococcus pneumoniae* and *Staphylococcus aureus* infections. J Antimicrob Chemother, 70(9), 2608–2617. https://doi.org/10.1093/jac/dkv163

Albada, H. B., Chiriac, A.-I., Wenzel, M., Penkova, M., Bandow, J. E., Sahl, H.-G., and Metzler-Nolte, N. (2012). Modulating the activity of short arginine-tryptophan containing antibacterial peptides with N-terminal metallocenoyl groups. Beilstein J. Org. Chem, 8(1), 1753–1764. https://doi.org/10.3762/bjoc.8.200

Alderden, R. A., Hall, M. D., and Hambley, T. W. (2006). The Discovery and Development of Cisplatin. J Chem Educ, 83(5), 728. https://doi.org/10.1021/ed083p728

Aller, I., Rouhier, N., and Meyer, A. J. (2013). Development of roGFP2-derived redox probes for measurement of the glutathione redox potential in the cytosol of severely glutathione-deficient rml1 seedlings. Front Plant Sci, 4, 506. https://doi.org/10.3389/fpls.2013.00506

Anagnostopoulos, C. and Spizizen, J. (1961). Requirements for transformation in *Bacillus subtilis*. J. Bacteriol, 81(5), 741–746. https://doi.org/10.1128/jb.81.5.741-746.1961

Angelucci, F., Sayed, A. A., Williams, D. L., Boumis, G., Brunori, M., Dimastrogiovanni, D., Miele, A. E., Pauly, F., and Bellelli, A. (2009). Inhibition of *Schistosoma mansoni* thioredoxin-glutathione reductase by Auranofin. Structural and kinetic aspects. J Biol Chem, 284(42), 28977–28985. https://doi.org/10.1074/jbc.M109.020701

Arnér, E. S. J., and Holmgren, A. (2005). Measurement of Thioredoxin and Thioredoxin Reductase. Curr Protoc Toxicol, *24*(1), 7.4.1-7.4.14. https://doi.org/10.1002/0471140856.tx0704s05

Arscott, L. D., Gromer, S., Schirmer, R. H., Becker, K., and Williams, C. H. (1997). The mechanism of thioredoxin reductase from human placenta is similar to the mechanisms of lipoamide dehydrogenase and glutathione reductase and is distinct from the mechanism of thioredoxin reductase from *Escherichia coli*. Proc Natl Acad Sci, 94(8), 3621–3626. https://doi.org/10.1073/pnas.94.8.3621

Aslam, B., Wang, W., Arshad, M. I., Khurshid, M., Muzammil, S., Rasool, M. H., Nisar, M. A., Alvi, R. F., Aslam, M. A., Qamar, M. U., Salamat, M. K. F., and Baloch, Z. (2018). Antibiotic resistance: a rundown of a global crisis. Infect Drug Resist, 11, 1645–1658. https://doi.org/10.2147/IDR.S173867

Augustus, A. M., Celaya, T., Husain, F., Humbard, M., and Misra, R. (2004). Antibiotic-sensitive TolC mutants and their suppressors. J Bacteriol, 186(6), 1851–1860. https://doi.org/10.1128/JB.186.6.1851-1860.2004

794 Baba, T., Ara, T., Hasegawa, M., Takai, Y., Okumura, Y., Baba, M., Datsenko, K. A., Tomita,
795 M., Wanner, B. L., and Mori, H. (2006). Construction of *Escherichia coli* K-12 in-frame,
796 single-gene knockout mutants: the Keio collection. Mol Syst Biol, 2, 2006.0008.
797 https://doi.org/10.1038/msb4100050
798 Bandow, J. E., Baker, J. D., Berth, M., Painter, C., Sepulveda, O. J., Clark, K. A., Kilty, I., and
799 VanBogelen, R. A. (2008). Improved image analysis workflow for 2-D gels enables
800 large-scale 2-D gel-based proteomics studies - COPD biomarker discovery study.
801 Proteomics, 8(15), 3030–3041. https://doi.org/10.1002/pmic.200701184
802 Bian, M., Fan, R., Zhao, S., and Liu, W. (2019). Targeting the Thioredoxin System as a
803 Strategy for Cancer Therapy. J Med Chem, 62(16), 7309–7321.
804 https://doi.org/10.1021/acs.jmedchem.8b01595
805 Butt, T. R., Edavettal, S. C., Hall, J. P., and Mattern, M. R. (2005). SUMO fusion technology
806 for difficult-to-express proteins. Protein Exp Purif, 43(1), 1–9.
807 https://doi.org/10.1016/j.pep.2005.03.016
808 Capparelli, E. V., Bricker-Ford, R., Rogers, M. J., McKerrow, J. H., and Reed, S. L. (2017).
809 Phase I Clinical Trial Results of Auranofin, a Novel Antiparasitic Agent. Antimicrob
810 Agents Chemother, 61(1). https://doi.org/10.1128/AAC.01947-16
811 Caroli, A., Simeoni, S., Lepore, R., Tramontano, A., and Via, A. (2012). Investigation of a
812 potential mechanism for the inhibition of SmTGR by Auranofin and its implications for
813 *Plasmodium falciparum* inhibition. Biochem Biophys Res Commun, 417(1), 576–581.
814 https://doi.org/10.1016/j.bbrc.2011.12.009
815 Cassetta, M. I., Marzo, T., Fallani, S., Novelli, A., and Messori, L. (2014). Drug repositioning:
816 auranofin as a prospective antimicrobial agent for the treatment of severe
817 staphylococcal infections. Biometals, 27(4), 787–791. https://doi.org/10.1007/s10534-
818 014-9743-6
819 Cha, Y., Erez, T., Reynolds, I. J., Kumar, D., Ross, J., Koytiger, G., Kusko, R., Zeskind, B.,
820 Risso, S., Kagan, E., Papapetropoulos, S., Grossman, I., and Laifenfeld, D. (2018).
821 Drug repurposing from the perspective of pharmaceutical companies. Br J Pharmacol,
822 175(2), 168–180. https://doi.org/10.1111/bph.13798
823 Debnath, A., Ndao, M., and Reed, S. L. (2012). Reprofiled drug targets ancient protozoans:
824 drug discovery for parasitic diarrheal diseases. Gut Microbes, 4(1), 66–71.
825 https://doi.org/10.4161/gmic.22596
826 Dooley, C. T., Dore, T. M., Hanson, G. T., Jackson, W. C., Remington, S. J., and Tsien, R. Y.
827 (2004). Imaging Dynamic Redox Changes in Mammalian Cells with Green Fluorescent
828 Protein Indicators. J Biol Chem, 279(21), 22284–22293.
829 https://doi.org/10.1074/jbc.M312847200

830 Dos Santos, H. F. (2014). Reactivity of auranofin with S-, Se- and N-containing amino acids.
831 Comput Theor Chem, 1048, 95–101. https://doi.org/10.1016/j.comptc.2014.09.005
832 Elkashif, A. and Seleem, M.N. (2020). Investigation of auranofin and gold-containing
833 analogues antibacterial activity against multidrug-resistant *Neisseria gonorrhoeae*. Sci
834 Rep, 10(1), 5602. https://doi.org/10.1038/s41598-020-62696-3.
835 Farha, M. A., and Brown, E. D. (2019). Drug repurposing for antimicrobial discovery. Nat
836 Microbiol, 4(4), 565–577. https://doi.org/10.1038/s41564-019-0357-1
837 Finkelstein, A. E., Walz, D. T., Batista, V., Mizraji, M., Roisman, F., and Misher, A. (1976).
838 Auranofin. New oral gold compound for treatment of rheumatoid arthritis. Ann Rheum
839 Dis, 35(3), 251–257. https://doi.org/10.1136/ard.35.3.251
840 Fuchs, B. B., RajaMuthiah, R., Souza, A. C. R., Eatemadpour, S., Rossoni, R. D., Santos, D.
841 A., Junqueira, J. C., Rice, L. B., and Mylonakis, E. (2016). Inhibition of bacterial and
842 fungal pathogens by the orphaned drug auranofin. Future Med Chem, 8(2), 117–132.
843 https://doi.org/10.4155/fmc.15.182
844 Gon, S., Faulkner, M. J., and Beckwith, J. (2006). *In Vivo* Requirement for Glutaredoxins and
845 Thioredoxins in the Reduction of the Ribonucleotide Reductases of *Escherichia coli*.
846 Antioxid Redox Signal, 8(5–6), 735–742. https://doi.org/10.1089/ars.2006.8.735
847 Gromer, S., Arscott, L. D., Williams, C. H., Schirmer, R. H., and Becker, K. (1998). Human
848 placenta thioredoxin reductase. Isolation of the selenoenzyme, steady state kinetics,
849 and inhibition by therapeutic gold compounds. J Biol Chem, 273(32), 20096–20101.
850 https://doi.org/10.1074/jbc.273.32.20096
851 Harbut, M. B., Vilchèze, C., Luo, X., Hensler, M. E., Guo, H., Yang, B., Chatterjee, A. K.,
852 Nizet, V., Jacobs, W. R., Schultz, P. G., and Wang, F. (2015). Auranofin exerts broad-
853 spectrum bactericidal activities by targeting thiol-redox homeostasis. Proc Natl Acad
854 Sci, 112(14), 4453–4458. https://doi.org/10.1073/pnas.1504022112
855 Hokai, Y., Jurkowicz, B., Fernández-Gallardo, J., Zakirkhodjaev, N., Sanaú, M., Muth, T. R.,
856 and Contel, M. (2014). Auranofin and related heterometallic gold(I)-thiolates as potent
857 inhibitors of methicillin-resistant *Staphylococcus aureus* bacterial strains. J Inorg
858 Biochem, 138, 81–88. https://doi.org/10.1016/j.jinorgbio.2014.05.008
859 Holmgren, A., and Björnstedt, M. (1995). Thioredoxin and thioredoxin reductase. Methods
860 Enzymol, 252, 199–208. https://doi.org/10.1016/0076-6879(95)52023-6
861 Humphreys, G., and Fleck, F. (2016). United Nations meeting on antimicrobial resistance.
862 Bull World Health Organ, 94(9), 638–639. https://doi.org/10.2471/BLT.16.020916
863 Hutchings, M. I., Truman, A. W., and Wilkinson, B. (2019). Antibiotics: past, present and
864 future. Curr Opin Microbiol, 51, 72–80. https://doi.org/10.1016/j.mib.2019.10.008
865

866 Hwang-Bo, H., Jeong, J.-W., Han, M. H., Park, C., Hong, S.-H., Kim, G.-Y., Moon, S.-K.,
867 Cheong, J., Kim, W.-J., Yoo, Y. H., and Choi, Y. H. (2017). Auranofin, an inhibitor of
868 thioredoxin reductase, induces apoptosis in hepatocellular carcinoma Hep3B cells by
869 generation of reactive oxygen species. Gen Physiol Biophys, 36(2), 117–128.
870 https://doi.org/10.4149/gpb_2016043
871 Jeon, K.-I., Byun, M.-S., and Jue, D.-M. (2003). Gold compound auranofin inhibits IκB kinase
872 (IKK) by modifying Cys-179 of IKKβ subunit. Exp Mol Med, 35(2), 61–66.
873 https://doi.org/10.1038/emm.2003.9
874 Kabuyama, Y., Kitamura, T., Yamaki, J., Homma, M. K., Kikuchi, S., and Homma, Y. (2008).
875 Involvement of thioredoxin reductase 1 in the regulation of redox balance and viability of
876 rheumatoid synovial cells. Biochem Biophys Res Commun, 367(2), 491–496.
877 https://doi.org/10.1016/j.bbrc.2007.12.178
878 Keseler, I. M., Mackie, A., Santos-Zavaleta, A., Billington, R., Bonavides-Martínez, C., Caspi,
879 R., Fulcher, C., Gama-Castro, S., Kothari, A., Krummenacker, M., Latendresse, M.,
880 Muñiz-Rascado, L., Ong, Q., Paley, S., Peralta-Gil, M., Subhraveti, P., Velázquez-
881 Ramírez, D. A., Weaver, D., Collado-Vides, J., … Karp, P. D. (2017a). The EcoCyc
882 database: reflecting new knowledge about *Escherichia coli* K-12. Nucleic Acids Res,
883 45(D1), D543–D550. https://doi.org/10.1093/nar/gkw1003
884 Koronakis, V. (2003). TolC - the bacterial exit duct for proteins and drugs. FEBS Letters,
885 555(1), 66–71. https://doi.org/10.1016/S0014-5793(03)01125-6
886 Lewis, P. J., and Marston, A. L. (1999). GFP vectors for controlled expression and dual
887 labelling of protein fusions in *Bacillus subtilis*. Gene, 227(1), 101–109.
888 https://doi.org/10.1016/S0378-1119(98)00580-0
889 Lu, J., and Holmgren, A. (2014). The thioredoxin antioxidant system. Free Radic Biol Med,
890 66, 75–87. https://doi.org/10.1016/j.freeradbiomed.2013.07.036
891 Lu, J., Vlamis-Gardikas, A., Kandasamy, K., Zhao, R., Gustafsson, T. N., Engstrand, L.,
892 Hoffner, S., Engman, L., and Holmgren, A. (2013). Inhibition of bacterial thioredoxin
893 reductase: An antibiotic mechanism targeting bacteria lacking glutathione. FASEB
894 Journal, 27(4), 1394–1403. https://doi.org/10.1096/fj.12-223305
895 Martinez, J. L., and Baquero, F. (2000). Mutation Frequencies and Antibiotic
896 Resistance. J. Antimicrob Agents, 44(7), 1771–1777.
897 https://doi.org/10.1128/AAC.44.7.1771-1777.2000
898 Marzo, T., Cirri, D., Pollini, S., Prato, M., Fallani, S., Cassetta, M. I., Novelli, A., Rossolini, G.
899 M., and Messori, L. (2018). Auranofin and its Analogues Show Potent Antimicrobial
900 Activity against Multidrug-Resistant Pathogens: Structure–Activity Relationships.
901 ChemMedChem, 13(22), 2448–2454. https://doi.org/10.1002/cmdc.201800498

902 Maurice, M. M., Nakamura, H., Gringhuis, S., Okamoto, T., Yoshida, S., Kullmann, F.,
903 Lechner, S., Van Der Voort, E. A. M., Leow, A., Versendaal, J., Muller-Ladner, U.,
904 Yodoi, J., Tak, P. P., Breedveld, F. C., and Verweij, C. L. (1999). Expression of the
905 thioredoxin-thioredoxin reductase system in the inflamed joints of patients with
906 rheumatoid arthritis. Arthritis Rheum, 42(11), 2430–2439. https://doi.org/10.1002/1529-
907 0131(199911)42:11<2430::AID-ANR22>3.0.CO;2-6
908 Messori, L., and Marcon, G. (2004). Gold complexes in the treatment of rheumatoid arthritis.
909 Met Ions Biol Syst, 41, 279–304. PMID: 15206120.
910 Meyer, A. J., and Dick, T. P. (2010). Fluorescent Protein-Based Redox Probes. Antioxid
911 Redox Signal, 13(5), 621–650. https://doi.org/10.1089/ars.2009.2948
912 Müller, A., Eller, J., Albrecht, F., Prochnow, P., Kuhlmann, K., Bandow, J. E., Slusarenko, A.
913 J., and Leichert, L. I. O. (2016). Allicin Induces Thiol Stress in Bacteria through S-
914 allylmercapto Modification of Protein Cysteines. J Biol Chem, 291(22), 11477-11490.
915 https://doi.org/10.1074/jbc.M115.702308
916 Müller, A., Hoffmann, J. H., Meyer, H. E., Narberhaus, F., Jakob, U., and Leichert, L. I.
917 (2013). Nonnative Disulfide Bond Formation Activates the 32-Dependent Heat Shock
918 Response in *Escherichia coli*. J Bacteriol, 195(12), 2807–2816.
919 https://doi.org/10.1128/JB.00127-13
920 Müller, A., Schneider, J. F., Degrossoli, A., Lupilova, N., Dick, T. P., and Leichert, L. I.
921 (2017). Systematic in vitro assessment of responses of roGFP2-based probes to
922 physiologically relevant oxidant species. Free Radic Biol Med, 106, 329–338.
923 https://doi.org/10.1016/j.freeradbiomed.2017.02.044
924 Munita, J. M., and Arias, C. A. (2016). Mechanisms of Antibiotic Resistance. Microbiol
925 Spectr., 4(2), 1–37. https://doi.org/10.1128/microbiolspec.VMBF-0016-
926 2015.Mechanisms
927 Neidhardt, F. C., Bloch, P. L., and Smith, D. F. (1974). Culture medium for enterobacteria. J
928 Bacteriol, 119(3), 736–747. https://doi.org/10.1128/jb.119.3.736-747.1974
929 Owings, J. P., McNair, N. N., Mui, Y. F., Gustafsson, T. N., Holmgren, A., Contel, M.,
930 Goldberg, J. B., and Mead, J. R. (2016). Auranofin and N- heterocyclic carbene gold-
931 analogs are potent inhibitors of the bacteria *Helicobacter pylori.* FEMS Microbiol Lett,
932 363(14), fnw148. https://doi.org/10.1093/femsle/fnw148
933 Rabilloud, T., Strub, J.-M., Luche, S., Dorsselaer, A. van, and Lunardi, J. (2001). A
934 comparison between Sypro Ruby and ruthenium II tris (bathophenanthroline
935 disulfonate) as fluorescent stains for protein detection in gels. Proteomics, 1(5),
936 699–704. https://doi.org/10.1002/1615-9861(200104)1:5<699::AID-
937 PROT699>3.0.CO;2-C
938

Rackham, O., Shearwood, A.-M. J., Thyer, R., McNamara, E., Davies, S. M. K., Callus, B. A., Miranda-Vizuete, A., Berners-Price, S. J., Cheng, Q., Arnér, E. S. J., and Filipovska, A. (2011). Substrate and inhibitor specificities differ between human cytosolic and mitochondrial thioredoxin reductases: Implications for development of specific inhibitors. Free Radic Biol Med, 50(6), 689–699. https://doi.org/10.1016/j.freeradbiomed.2010.12.015

Rigobello, M. P., Folda, A., Baldoin, M. C., Scutari, G., and Bindoli, A. (2005). Effect of Auranofin on the mitochondrial generation of hydrogen peroxide. Role of thioredoxin reductase. Free Radic Res, 39(7), 687–695. https://doi.org/10.1080/10715760500135391

Rigobello, M. P., Scutari, G., Folda, A., and Bindoli, A. (2004). Mitochondrial thioredoxin reductase inhibition by gold(I) compounds and concurrent stimulation of permeability transition and release of cytochrome c. Biochem Pharmacol, 67(4), 689–696. https://doi.org/10.1016/j.bcp.2003.09.038

Saccoccia, F., Angelucci, F., Boumis, G., Brunori, M., Miele, A. E., Williams, D. L., and Bellelli, A. (2012). On the mechanism and rate of gold incorporation into thiol-dependent flavoreductases. J Inorg Biochem, 108, 105–111. https://doi.org/10.1016/j.jinorgbio.2011.11.005

Scharf, C., Riethdorf, S., Ernst, H., Engelmann, S., Völker, U., and Hecker, M. (1998). Thioredoxin is an essential protein induced by multiple stresses in Bacillus subtilis. J Bacteriol, 180(7), 1869–1877. https://doi.org/10.1128/JB.180.7.1869-1877.1998

Senges, C. H. R., Stepanek, J. J., Wenzel, M., Raatschen, N., Ay, Ü., Märtens, Y., Prochnow, P., Hernández, M. V., Yayci, A., Schubert, B., Janzing, N. B. M., Warmuth, H. L., Kozik, M., Bongard, J., Alumasa, J. N., Albada, B., Penkova, M., Lukežič, T., Sorto, N. A., … Bandow, J. E. (2020). Comparison of Proteomic Responses as Global Approach to Antibiotic Mechanism of Action Elucidation. Antimicrob Agents Chemother, 65(1), e01373-20. https://doi.org/10.1128/AAC.01373-20

Storz, G., and Tartaglia, L. A. (1992). OxyR: a regulator of antioxidant genes. J Nutr, 122(3 Suppl), 627–630. https://doi.org/10.1093/jn/122.suppl_3.627

Storz, G., Tartaglia, L. A., and Ames, B. N. (1990). The OxyR regulon. Anton Leeuw Int J G, 58(3), 157–161. http://doi.org/10.1007/BF00548927

Stulke, J., Hanschke, R., and Hecker, M. (1993). Temporal activation of β-glucanase synthesis in Bacillus subtilis is mediated by the GTP pool. J Gen Microbiol, 139(9), 2041–2045. https://doi.org/10.1099/00221287-139-9-2041

974 Thangamani, S., Mohammad, H., Abushahba, M. F. N., Sobreira, T. J. P., Hedrick, V. E.,
975 Paul, L. N., and Seleem, M. N. (2016). Antibacterial activity and mechanism of action of
976 auranofin against multi-drug resistant bacterial pathogens. Sci Rep, 6, 22571.
977 https://doi.org/10.1038/srep22571
978 Uziel, O., Borovok, I., Schreiber, R., Cohen, G., and Aharonowitz, Y. (2004). Transcriptional
979 regulation of the *Staphylococcus aureus* thioredoxin and thioredoxin reductase genes in
980 response to oxygen and disulfide stress. J Bacteriol, 186(2), 326–334.
981 https://doi.org/10.1128/jb.186.2.326-334.2004
982 Wang, H.-H., Su, C.-H., Wu, Y.-J., Lin, C.-A. J., Lee, C.-H., Shen, J.-L., Chan, W.-H., Chang,
983 W. H., and Yeh, H.-I. (2012). Application of Gold in Biomedicine: Past, Present and
984 Future. Int J Gerontol, 6(1), 1–4. https://doi.org/10.1016/j.ijge.2011.09.015
985 Wenzel, M., Patra, M., Albrecht, D., Chen, D. Y.-K., Nicolaou, K. C., Metzler-Nolte, N., and
986 Bandow, J. E. (2011). Proteomic signature of fatty acid biosynthesis inhibition available
987 for in vivo mechanism-of-action studies. Antimicrob Agents Chemother, 55(6), 2590–
988 2596. https://doi.org/10.1128/AAC.00078-11
989 Wenzel, M., Patra, M., Senges, C. H. R., Ott, I., Stepanek, J. J., Pinto, A., Prochnow, P.,
990 Vuong, C., Langklotz, S., Metzler-Nolte, N., and Bandow, J. E. (2013). Analysis of the
991 mechanism of action of potent antibacterial hetero-tri-organometallic compounds: a
992 structurally new class of antibiotics. ACS Chem Biol, 8(7), 1442–1450.
993 https://doi.org/10.1021/cb4000844
994

995 **SUPPLEMENTARY DATA**

996 **Supplemental Table S1: Oligonucleotides used in this study.**

Oligonucleotide	Sequence (5′ → 3′)
AI001_for	GAACAGATTGGAGGTGGCACGACCAAAC
AI002_rev	GCGACTCGAGTTATTTTGCGTCAGCTAAAC
AI003_SUMO_for	GCGTCATATGGGTCATCACCATCATC
AI004_SUMO_rev	GGTCGTGCCACCTCCAATCTGTTC
MM001_for	AACAGATTGGAGGTGTGTCAGAAGAAAAAATTTAT GACGTG
MM002_rev	GCGCCTCGAGTTATTTTAAGGTTTTCAGCGTTTCTTG GAGC
MM004_SUMO_rev	TTTTTCTTCTGACACACCTCCAATCTGTTCGCGGTGAG
MV001_for	CATCATATGAGCGATAAAATTATTCACC
MV002_rev	GAACTCGAGTTACGCCAGGTTAGCGTCGAGG
LQB001_for	AAACATATGATGGCTATCGTAAAAGCAA
LQB002_rev	AAAGGATCCTTAAAGATGTTTGTTTACAA
JY001_for	AAAGGTACCATGGTTAGCAAAGGC
JY002_rev	AAAAAGCTTTTACTTGTACAGTTCATCCATG

997
998
999 **Supplemental Table S2: List of marker protein spots induced after treatment with Auranofin in**
1000 ***E. coli* MG1655.** Bold proteins met criteria for MS identification, proteins denoted with (excl.) were
1001 matched by the search engine, but were excluded, as they did not meet the criteria for Peptides (at least
1002 3), Fragments (at least 5), Coverage % (at least 10), or gel position was inconsistent with theoretical
1003 MW or pI. N/A: the search engine did not produce a match. EcoCyc Accession Number and function
1004 obtained from the EcoCyc database (Keseler et al., 2017). Peptides: number of peptides annotated by
1005 the search engine, Fragments: number of product ions annotated by the search engine. Coverage:
1006 coverage of the protein sequence by the annotated peptides in %.
1007

Spot ID	Regulation factor	Protein	EcoCyc Accession Number	Function	theoretical MW [Da]	theoretical pI	Peptides	Fragments	Coverage %
25	3.2	**SucA**	EG10979	2-oxoglutarate decarboxylase, thiamine-requiring	104995	6.0	15	81	18.3
44	4.1	**HtpG**	EG10461	chaperone protein HtpG	71378	4.9	39	296	42.0
		CsiR (excl.)	EG12386	DNA-binding transcriptional repressor GlaR	24974	6.2	5	15	18.2
		YciH (excl.)	EG11128	putative translation factor	11389	9.8	4	13	26.9
		AroK (excl.)	EG10081	shikimate kinase 1	19526	5.1	2	5	17.3
239	2.0	**RpiA**	EG11443	ribose-5-phosphate isomerase A	22845	5.0	4	21	17.4
326	2.4	EptA (excl.)	EG11613	phosphoethanolamine transferase EptA	61627	6.4	2	9	9.5
328	2.4	**MoaB**	EG11596	protein MoaB	18653	5.7	6	83	25.3
347	3.2	**Bfr**	EG10113	bacterioferritin	18483	4.5	3	18	11.4

Spot ID	Regulation factor	Protein	EcoCyc Accession Number	Function	theoretical MW [Da]	theoretical pI	Peptides	Fragments	Coverage %
357	2.3	N/A							
374	2.3	FtsK (excl.)	G6464	cell division DNA translocase FtsK	146571	4.7	5	25	2.5
497	2.3	**AhpC**	EG11384	alkyl hydroperoxide reductase, AhpC component	20748	4.8	5	32	21.9
537	3.7	N/A							
606	4.4	YbcJ (excl.)	EG12879	putative RNA-binding protein YbcJ	7384	8.3	3	19	4.3
		XapR (excl.)	EG11146	DNA-binding transcriptional activator XapR	33605	9.1	2	7	12.2
620	2.7	**MglB**	EG10593	D-galactose/methyl-galactoside ABC transporter periplasmic binding protein	35690	5.6	23	156	50.3
638	2.7	N/A							
662	3.9	**YeaG**	G6969	protein kinase YeaG	74433	5.5	25	160	32.3
690	2.1	**CysN**	EG10194	sulfate adenylyltransferase subunit 1	52526	4.8	45	336	47.8
		GpmM	EG12296	2,3-bisphosphoglycerate-independent phosphoglycerate mutase	56158	5.0	8	35	13.6
		YedJ (excl.)	EG12710	putative HD superfamily phosphohydrolase YedJ	25888	5.9	4	14	17.3
692	2.6	**GpmM**	EG12296	2,3-bisphosphoglycerate-independent phosphoglycerate mutase	56158	5.0	25	168	21.6
		IhfA (excl.)	EG10440	integration host factor subunit α	11346	9.9	2	7	19.2
718	6.1	**Pgk**	EG10703	phosphoglycerate kinase	41092	4.9	7	41	17.6
752	7.0	CueO (excl.)	EG12318	multicopper oxidase CueO	56519	6.3	5	46	9.7
		Php (excl.)	G7731	putative hydrolase	32894	5.1	4	15	20.9
754	7.2	**Lpd**	EG10543	lipoamide dehydrogenase	50656	5.7	10	93	25.7
		MalI (excl.)	EG10557	DNA-binding transcriptional repressor MalI	36602	6.5	7	20	28.1
756	4.0	**Lpd**	EG10543	lipoamide dehydrogenase	50656	5.7	10	64	28.5
		Amn	EG10039	AMP nucleosidase	53961	5.9	11	49	19.8
		AtpA	EG10098	ATP synthase F1 complex subunit α	55187	5.7	6	38	10.7
757	4.1	Tcyj (excl.)	G7039	cystine ABC transporter periplasmic binding protein	29021	6.2	4	21	12.0
		MepM (excl.)	EG10013	peptidoglycan endopeptidase MepM	49027	9.8	6	20	13.9
758	15.0	**AtpA**	EG10098	ATP synthase F1 complex subunit α	55187	5.7	12	74	18.7
		Amn (excl.)	EG10039	AMP nucleosidase	53961	5.9	7	31	9.1
763	4.6	**Amn**	EG10039	AMP nucleosidase	53961	5.9	8	39	14.9
		AtpA	EG10098	ATP synthase F1 complex subunit α	55187	5.7	13	64	21.8
		CueO	EG12318	multicopper oxidase CueO	56519	6.3	3	25	11.0
		IbpB (excl.)	EG11535	small heat shock protein IbpB	16083	5.0	4	12	19.7

Spot ID	Regulation factor	Protein	EcoCyc Accession Number	Function	theoretical MW [Da]	theoretical pI	Peptides	Fragments	Coverage %
764	4.9	AtpA (excl.)	EG10098	ATP synthase F1 complex subunit α	55187	5.7	6	25	9.1
		ArgA (excl.)	EG10063	N-acetylglutamate synthase	49164	6.1	5	20	8.5
		PyrC (excl.)	EG10806	dihydroorotase	38802	5.8	3	14	8.6
782	4.0	**Gor**	EG10412	glutathione reductase	48741	5.6	16	91	35.1
		Mpl	EG12440	UDP-N-acetylmuramate—L-alanyl-γ-D-glutamyl-meso-2,6-diaminoheptanedioate ligase	49842	5.5	13	57	19.9
		GlmM	EG11553	phosphoglucosamine mutase	47513	5.6	9	50	20.0
		PhoA	EG10727	alkaline phosphatase	49408	5.7	11	45	31.2
806	3.9	**NemA**	G6890	N-ethylmaleimide reductase	39492	5.8	7	52	19.7
		YaiI (excl.)	G6230	DUF188 domain-containing protein YaiI	16958	5.4	5	18	22.4
816	3.0	**PyrC**	EG10806	dihydroorotase	38802	5.7	17	131	21.8
		YqhD	G7564	NADPH-dependent aldehyde reductase YqhD	42070	5.7	11	65	21.7
852	3.0	YoaA (excl.)	G6992	ATP-dependent DNA helicase YoaA	70333	6.7	5	21	6.4
		PstS (excl.)	EG10734	phosphate ABC transporter periplasmic binding protein	37001	9.0	3	12	9.0
		DnaE (excl.)	EG10238	DNA polymerase III subunit α	129822	5.0	5	22	3.2
		PaaE (excl.)	G6713	phenylacetyl-CoA 1,2-epoxidase, reductase subunit	39294	5.9	3	11	4.8
859	3.6	**PykF**	EG10804	pyruvate kinase 1	50697	5.7	10	61	17.2
		AhpF (excl.)	EG11385	alkyl hydroperoxide reductase, AhpF component	56142	5.3	3	17	5.8
860	3.6	**AhpF**	EG11385	alkyl hydroperoxide reductase, AhpF component	56142	5.3	22	168	36.5
		LeuA	EG11226	2-isopropylmalate synthase	57262	5.4	19	126	31.5
		PyrF (excl.)	EG10809	orotidine-5'-phosphate decarboxylase	26333	5.8	4	14	24.9

1008